UNIVERSITA' DEGLI STUDI DI MILANO-BICOCCA

FACOLTA' DI MEDICINA E CHIRURGIA

CORSO DI DOTTORATO IN TECNOLOGIE BIOMEDICHE (XXV ciclo)

PET IMAGING FOR EVALUATION OF INFLAMMATORY RESPONSE IN A MURINE MODEL OF ACUTE RESPIRATORY FAILURE

TUTORE: Chiar.ma Prof.ssa Cristina MESSA

COTUTORE: Dott. Giacomo BELLANI

COORDINATORE: Prof.ssa Marina DEL PUPPO

Tesi di Dottorato di:

Vanessa ZAMBELLI

Matr. n° 734498

Anno accademico 2011/2012

Table of contents

Abstract

ABSTRACT

Background: Acute Respiratory Distress Syndrome (ARDS) is a life-threatening form of acute respiratory failure, with a still high mortality. Aspiration pneumonitis is a clinical disorder that, entailing a direct lung injury, is associated to ARDS. It is characterized by an acute inflammatory response with neutrophilic recruitment into the lung and a late fibrotic evolution of injury. This study investigates whether the use of PET could allow to monitor this inflammatory response and its correlation with the later fibroproliferative phase in an experimental model of acute respiratory failure. Since to date no specific therapeutic strategies are available for ARDS patients, we tested the effects of exogenous surfactant treatment on lung injury evolution, by monitoring it with CT-PET imaging.

Methods: Hydrochloric acid (0,1M) was instilled (1,5 ml/kg) into the right bronchus of mice. The study was divided into three parts.

Time-course experiment: four groups of mice underwent micro-CT and micro-PET scans and sacrificed at different time point (6hrs, 24 hrs, 48 hrs and 7 days after surgery) to assess arterial blood gases, histology and bronchoalveolar lavage (BAL).

Long-term experiment: one group of mice underwent a micro-CT scan 1 hour after lung injury and a series of [^{18}F]FDG-PET at the same time points. 21 days after respiratory static compliance was measured and lung tissue was collected in order to measure the OH-proline content.

Treatment experiment: two groups of mice were treated with exogenous surfactant (Curosurf ®) or vehicle (sterile saline 0.9 %) three hours after HCl instillation. Animals underwent micro-CT and a series of micro-PET scans. 21

days after they were sacrificed to measure lung mechanics and collagen deposition.

Results: Histological analysis showed a rapid recruitment of neutrophils into the damaged lung 6 hours after injury, with a peak after 24 hours. Macrophages, as expected, reached the peak after 48 hours. [^{18}F]FDG signal, as inflammation marker, showed similar time course to that of recruited inflammatory cells (sum of two cell types). Mice that were sacrificed 21 days after the surgery were characterized by a correlation between a reduced respiratory static compliance and a high PET signal 7 days after lung injury. PET signal correlated also with collagen content. This correlation was confirmed in treatment experiment, in which we found that exogenous surfactant administration improved lung fibrotic evolution, by reducing collagen deposition.

Conclusions: This study demonstrated the possibility to use PET imaging to follow the inflammatory response also in longitudinal studies. Moreover a correlation between a persistence of inflammatory process and fibrotic evolution was showed. We speculate that it is possible that acute treatments of the inflammation capable of reducing the fibroproliferative process, could be monitored using the FDG-PET method.

Introduction

INTRODUCTION

1. ARDS

1.1 Definition

Acute Respiratory Distress Syndrome (ARDS) is a serious form of acute respiratory failure that affects both medical and surgical patients (1). In 1967 Ashbaugh (2) introduced the term "Respiratory Distress Syndrome" in order to describe 12 patients with acute onset of tachipnea, diffuse alveolar infiltration, decreased lung compliance and hypoxemia. In 1994 a new definition was established by the American-European Consensus Conference (AECC) (3) aimed at facilitating the study of the epidemiology, pathophysiology and the treatment of ARDS. In this conference the following criteria were established:

- acute onset,

- bilateral infiltrates on chest radiography,

- pulmonary artery wedge pressure lower than 18mmHg or absence of left atrial hypertension,

- ALI (Acute Lung Injury) if PaO2/FiO2 is lower than 300,

- ARDS if PaO2/FiO2 is lower than 200.

In general, considering the complexity of this disease it has been stated that ARDS is an acute (rapid onset) syndrome (collection of symptoms) that affects the lungs diffusely and results in a severe oxygenation defect, but not due to heart failure.

This definition presents two disadvantages: patients with different conditions are gathered together with a high heterogeneity in clinical trials, and it is an easy but vague definition. For this reason, recently, in 2011, a group of experts developed the so called "Berlin definition" (4) in order to revise the ARDS definition. Several changes were made, in particular the acute time frame was specified, the chest radiography criteria were clarified and the ALI/ARDS distinction was modified: the term ALI was removed and 3 subgroups of ARDS were created depending on the severity (mild, moderate and severe).

1.2 Epidemiology

5% of hospitalized, mechanically ventilated patients suffer from ARDS (5), but the accurate estimation of the incidence is not available because of the heterogeneity of causes. Moreover the incidence differs between different geographical areas. In USA, perspective studies (6, 7) estimate almost 70 cases/100000 person-years, whereas other countries show lower rate.

ARDS is associated with a still high mortality, almost 40% (6). In the Berlin definition, mild ARDS patients show 27% mortality, while moderate and severe ARDS patients 32% and 45% respectively (4). Mortality usually occurs because of multiorgan dysfunction, even if worsening oxygenation remains an important risk factor for ARDS mortality (8, 9). Two types of clinical disorders are associated with ARDS: direct and indirect lung injury. Among the direct injuries the most common are bacterial, viral or fungal pneumonia, aspiration of gastric contents, pulmonary contusion and toxic inhalational injury. Severe sepsis and severe trauma with hemorrhage and shock are the common cause of indirect lung injury, apart from acute pancreatitis and blood transfusions (4).

1.3 Pathogenesis

The pathology usually advances through three stages: exudative, proliferative and sometimes it progresses towards the fibrotic phase (10).

I.   EXUDATIVE PHASE: concurs with the acute inflammatory stage, and it is characterized by an intense alteration of barrier permeability with accumulation of protein-rich fluid; a massive release of pro-inflammatory cytokines and neutrophils influx.

II. PROLIFERATIVE PHASE: its development occurs in one week after lung insult and consists in edema reabsorption, wall thickening of alveolar capillary, proliferation of type II pneumocytes and early signs of fibrosis are visible.

III. FIBROTIC PHASE: defined by an important collagen deposition and by a decrease in lung mechanical properties.

Exudative phase

This phase occurs immediately after the injury and begins with the lung endothelial and epithelial injury, known as the most important initial cause of ARDS (11). It leads to an increase of lung vascular permeability with the ensuing accumulation of protein-rich pulmonary edema. The lung endothelium may be injured by several mechanisms, but the most known is neutrophil-dependent lung injury. Neutrophils, once activated, lead to secretion of many inflammatory and toxic mediators that induce an alteration in endothelial barrier function (11) and they can also migrate in epithelium and damage it. The degree of alveolar epithelial injury is a predictor of the ARDS outcome (12, 13).
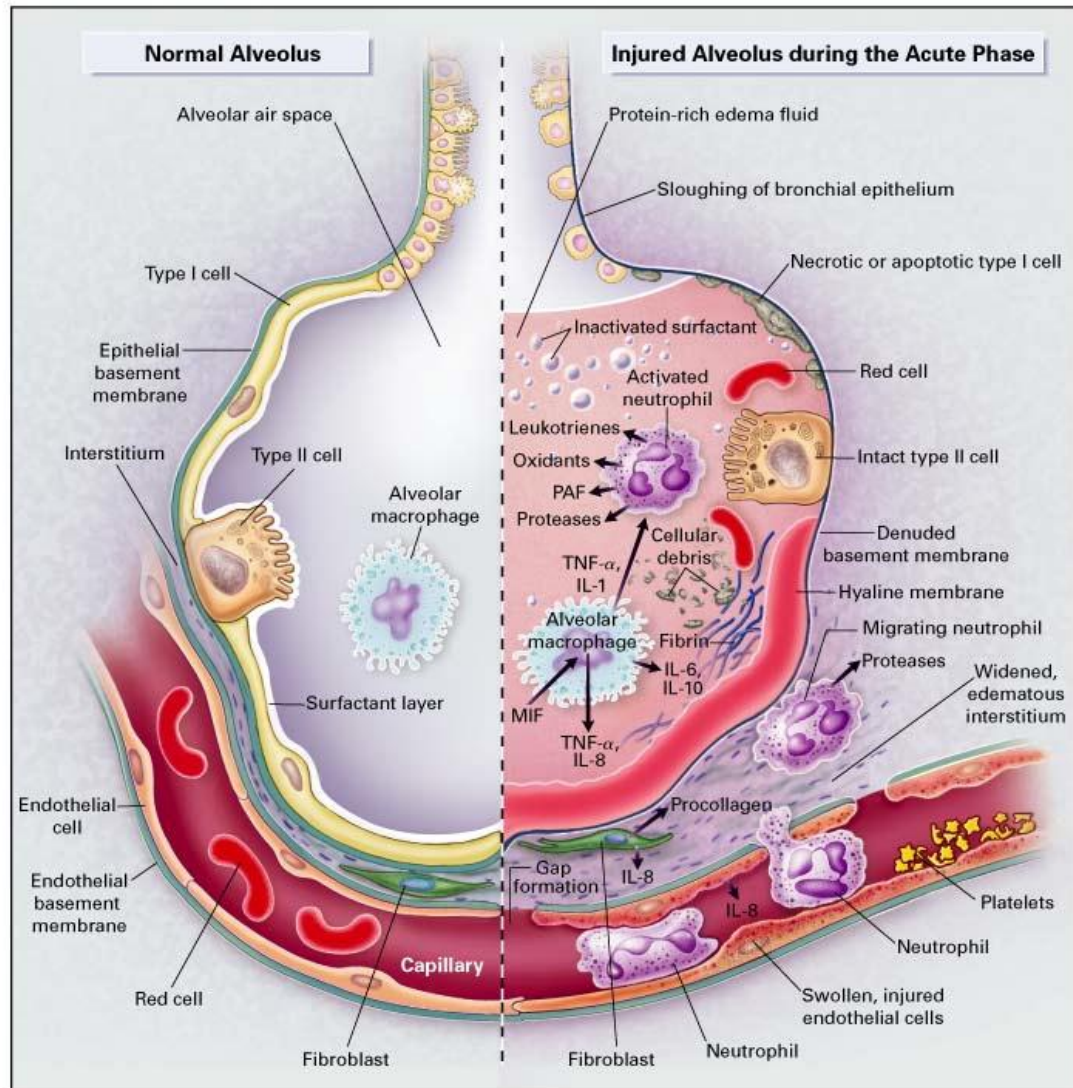
The Normal Alveolus (Left-Hand Side) and the Injured Alveolus in the Acute Phase of Acute Lung Injury and the Acute Respiratory Distress Syndrome (Right-Hand Side). Reproduced with permission from (**Ware LB, Matthay MA. N Engl J Med 2000;342:1334-1349**), Copyright Massachusetts Medical Society

Proliferative phase

In this phase alveolar spaces are full of mesenchymal cells and their products, moreover new vessels are formed. Soluble proteins are removed via diffusion process and unsoluble ones are removed via phagocytosis performed by macrophages. Type II pneumocytes begin to proliferate and differentiate

towards type I pneumocytes, in an attempt to re-establish the normal alveolar architecture and the fluid transport.
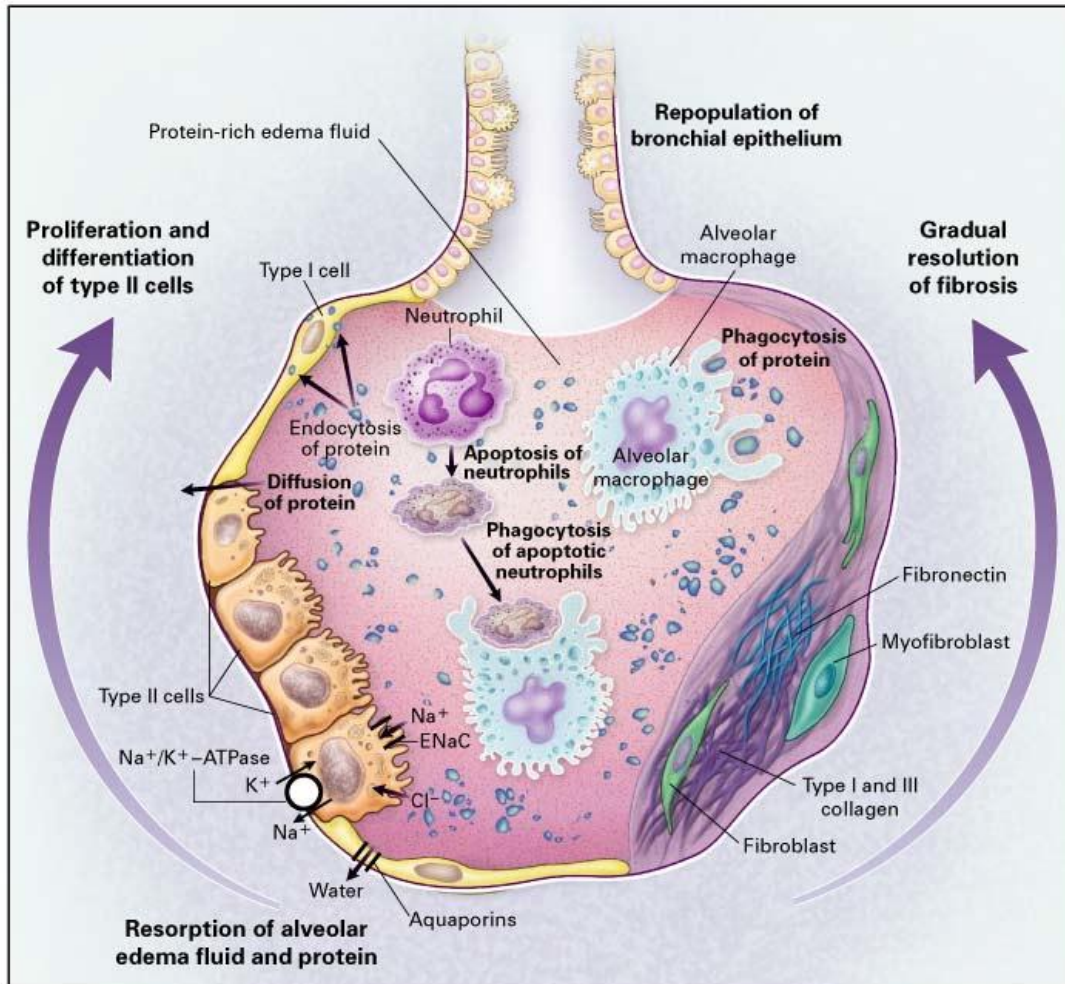
Mechanisms Important in the Resolution of Acute Lung Injury and the Acute Respiratory Distress Syndrome. Reproduced with permission from (**Ware LB, Matthay MA. N Engl J Med 2000;342:1334-1349**), Copyright Massachusetts Medical Society

Fibrotic phase

In some patients the course of the pathology is not complicated and terminates with the injury resolution. But sometimes the proliferative phase progresses to a fibrotic stage, characterized by an intense collagen deposition, that alters the

physiologic ventilation/perfusion ratio. Fibrosis is responsible also for the pulmonary stiffness and the consequent impairment of mechanical properties, that lead to respiratory muscle weariness, reduction of tidal volume and worsening of gas exchange.

1.3.1 Neutrophils

Neutrophils are polymorphonuclear cells (PMNs) are the most abundant circulating leucocytes and are important responsible for the innate immunity (14). Because of their physiological function, they are highly motile and are able to respond to the finest chemotactic signals under adverse conditions (15). Once recruited to the site of inflammation they release preformed enzymes, cytotoxic products, such as reactive oxygen species, cationic peptides and eicosanoids (16). In certain conditions (ARDS, Chronic Obstructive Pulmonary Disease-COPD, asthma and rheumatoid arthritis) neutrophilic inflammation becomes autonomous, chronic and injurious to healthy tissue (18). Of course neutrophils are fundamental for host defense and for the preservation of health, but their uncontrolled and over-activation leads to serious tissue damage since they release several cytotoxic and immune cell-activating agents (16) and appear to contribute to the oxidant-induced injury and loss of epithelial integrity (17, 19). Indeed they play a key role in the progression of ARDS, their activation seems to be the central event of the inflammatory response that characterizes acute lung injury (18). ARDS has been described also in neutropenic patients (20), but neutrophils remain the major contributor to lung inflammation. In fact neutrophils release growth factors, cytokines and chemokines, that enhance the inflammatory response (21). In many patients with lung injury a deterioration of pulmonary function was found as soon as neutropenia was finished (22).

Different studies (23-25) demonstrated that the concentration of neutrophils in bronchoalveolar lavage (BAL) from patients with ARDS correlates with the severity of ARDS and with outcome.

Recruitment of neutrophils into the lung.

During ARDS neutrophils are the earliest immune cells recruited to the site of injury, involving a transient leukopenia (26). The process of recruitment takes place after the release of chemoattractants by resident cells and changes in the biomechanical and adhesive properties of neutrophils (21). The most important pro-inflammatory cytokines are interleukin 1-b (IL-1b) and tumor necrosis factor-alpha (TNF-a). These two cytokines are produced mainly by resident alveolar macrophages and induce the production of many chemotactic factors, such as IL-8, the major chemotactic factor for recruitment of neutrophils (27). IL-8 induces the activation of neutrophils (28) and up-regulates adhesion molecules; moreover it facilitates neutrophilic migration trough the endothelium (29). Once activated, neutrophils then extravasate in postcapillary venules through a process entailing a cascade of sequential cell-adhesion and cell-activation, such as tethering, rolling and migration (30-32), that is mediated by selectins, integrins and chemokines (16). Recruitment, activation and adhesion are important processes for the development of lung injury (33, 34), since the release of cytotoxic agents occurs when neutrophils are adherent to endothelium and epithelium (35). The inflammatory cascade induces also the activation of the coagulation system, which in turn feeds the inflammatory response by enhancing production of further cytokines and recruitment of inflammatory cells.

1.3.2 Macrophages

Macrophages were described for the first time by Metchnikoff in the 1880s. They are large mononuclear phagocytic cells and their predominant function is the host defense (36). Macrophages are antigen-presenting cells and participate in humoral and cell-mediated immunity (37). Their precursors are generated in bone marrow (37), then they are released into the blood stream as monocytes and differentiate into macrophages or dendritic cells into tissues (36). Two type of macrophages exist: tissue-resident and recruited macrophages. The former type includes specialized subpopulations based on anatomical location (such as alveolar macrophages in the lung or Kupffer cells in the liver) and forms a constant pool of cells that are constituent part of tissue homeostasis. The latter type is recruited after a stimulus and plays important role in acute inflammatory response (38). Macrophages are further divided into two functional groups based on their activation state (39): M1 and M2. M1 macrophages have pro-inflammatory properties and mediate host defense against bacteria, viruses and protozoa. Whereas M2 macrophages have anti-inflammatory properties and are involved in wound healing (40). Macrophage activation towards a particular state depends on the presence of activators or cytokines. Among a wide range of factors, responsible for macrophage activation, L-arginine metabolism plays a central role in macrophage signaling between M1 and M2. M1 macrophages increase NO (nitric oxide) production and bacterial killing, if nitric oxide synthase (NOS) activity increases. On the other hand, if arginase 1 activity increases and NOS activity decreases, M2 macrophages begin to produce proliferation-inductor molecules or proline, a component of collagen, promoting tissue repair (40).

Role of macrophages during lung injury

As already mentioned, the first phase following lung injury is characterized by an inflammatory response. This process involves immune system and components of the coagulation cascade (36). In this inflammatory context macrophages play a key role in the recruitment of neutrophils to injury site. A recent study (41) with two-photon imaging has demonstrated an interesting cross-talk between monocytes and neutrophils. A decrease in neutrophil recruitment in the lung was revealed after monocytes depletion. It is well known that macrophages are important cells in the progression of ARDS. Alveolar macrophages could secrete many pro-inflammatory mediators (IL-1β, IL-4 and IL-13) and growth factors, such as TGF-β (transforming growth factor- beta), TGF-α, PDGF (platelet-derived growth factor) and FGF (fibroblast growth factor). These growth factors are involved in the progression of fibroproliferative lung disorders, since they induce mesenchymal cells migration, proliferation and ECM (extracellular matrix) deposition (42). An important role of this first part of the process is to form a provisional matrix, composed by fibrin, fibronectin and platelets (36). Proliferation and migration of different cell types are typical events of the second phase. Macrophages stimulate fibroblasts to differentiate into myofibroblasts. Fibroblasts and myofibroblasts are assigned to collagen deposition and to the formation of injury-associated extracellular matrix. If the injury does not alter the basement membrane integrity, a normal ECM has been deposited, but if the basement membrane is irreparably damaged, then scarring occurs, with inevitable structural alterations (36). In the last phase the down-regulation of molecular injury associated-processes generally occurs.

But after a persistent smoldering inflammation an inadequate regulation/suppression of the reaction may happen. Failure to resolve inflammation can leave residual impairment and often leads to tissue fibrosis (42). Pulmonary fibrosis is seen in 55% of death case, suggesting that dysregulated repair contributes to morbidity and mortality in ARDS patients (43).

1.3.3 Surfactant

Surfactant is a lipid-protein complex synthesized and secreted from alveolar type II pneumocytes (44). Its main function is to reduce surface tension in the lung preventing the lung from collapsing at resting transpulmonary pressures (44). Endogenous surfactant is constituted by 90% lipids (phospholipids, neutral lipids) and 10% proteins (specific surfactant proteins, SP-A, SP-B, SP-C and SP-D). Saturated phosphatidylcoline (Sat.PC) is the main surface active component (44). It is synthesized in the endoplasmic reticulum of the type II pneumocytes and then secreted into alveoli. Its uncommon characteristic conformation with two saturated residues (mainly palmitate residues) avoids alveolar collapse during expiration and permits alveolar expansion during inspiration (45). Type II cells are the only cells involved in modulation of surfactant synthesis, secretion, uptake, and catabolism. Endogenous surfactant, once secreted, settles as layers on the alveolar surface and these forms are called large aggregates (LA), that represent the functional component of endogenous surfactant (46). During normal respiratory cycle, LA surfactant undergo a conversion into nonfunctional small aggregates (SA) (46). Alveolar macrophages contribute to surfactant homeostasis by recycling or degrading SA (47). Thus the surface film is dynamic with new surfactant continuously being produced, re-uptaken, degraded and or recycled (47).

The interactions between the components of pulmonary surfactant are fundamental to maintain normal lung function (44). Surfactant allows collapsed alveoli to open even at low inspiratory pressure and to keep alveolar size during inflation (44). Surface tension is defined by the Law of Young and Laplace, $\Delta P = 2\sigma/R$, where P is the pressure, σ is the surface tension and R is the alveolar radius (44). This equation describes the property of surfactant of reducing surface tension with a decrease in alveolar radius, in order to keep the surface tension/radius ratio of alveoli constant thus preventing epithelial overstretching (48).

Surfactant alterations in lung injury contribute to the pathophysiology of ARDS. Indeed altered surfactant function has been found in autopsy specimens of ARDS patients. In particular an increased surface compressibility of surfactant recovered from ARDS patient was observed (44).

During ARDS several mechanisms lead to disruption of endogenous surfactant system: damage to alveolar type II pneumocytes, leakage into airspace of serum proteins, endopeptidase, phospholipase A2 and mechanical ventilation (49). If alveolar type II cells are altered, then abnormal synthesis and secretion of surfactant occurs. Whole surfactant metabolism is altered and alveolar surfactant pool sizes and phospholipid composition could change (44). The presence of serum proteins in alveolar space induces disaggregation of the surfactant structures, since they facilitate the transformation of the active LA to SA with lower surfactant capacity (50). Among serum proteins, fibrin degradation products and fibrinogen have a potent inhibitory action. Proteins compete with endogenous surfactant for the surface thus interfering with layer formation (44). Other substances are able to inactivate surfactant: lipid

peroxidation products (such as oxygen radicals) and phospholipases (44). In particular phospholipases can interfere with surfactant function by decreasing alveolar lipid levels and/or by inducing the production of lysophosphatidylcholine, that damages the epithelium and impairs surface properties of surfactant (44).

In addition to clinical observations, several acute lung injury models have confirmed the correlation between the surfactant dysfunction and the worsening of physiologic parameters. Maruscak et al. (51) demonstrated, in a rat model of VILI (Ventilation Induced Lung Injury), that the alterations to surfactant system precede lung dysfunction. They observed that the primary cause of surfactant impairment is due to serum proteins, but also the hydrophobic components of surfactant contribute to the dysfunction.

1.4 Experimental model

The first acid aspiration-induced death dates at 1848, this case was associated to general anesthesia and it was published on Lancet (52). In 1946 Mendelson described, for the first time, the aspiration pneumonitis in patients that underwent general anesthesia for obstetrical interventions (53). He learned that the gastric content aspiration, such as the same volume of 0.1N HCl, could induce a severe pneumonitis, thus demonstrating a strong role played by acid content in the pathogenesis of pneumonitis. After this discovery several studies were aimed at creating animal models able to mimic faithfully the human conditions. There is no model that reproduces perfectly the human pathology, but these models have allowed to describe the time course of the injury development, the bio-humoral and biochemical mechanisms in order to delineate the pathogenesis (54-56). The acid aspiration model is characterized by a biphasic process. The first phase occurs in the first two hours after instillation/aspiration and consists in the direct chemical injury acid-mediated on the pulmonary parenchyma and epithelial and endothelial barrier, leading to increase of vascular permeability. The second phase composed of a delayed (four hours after injury) inflammatory injury mediated by neutrophils. Indeed it is associated to a presence of neutrophilic infiltrate in alveoli and pulmonary interstitium (54-56).

Our group has recently developed a murine model of unilateral acid induced lung injury (57), by characterizing it from functional, biochemical and morphologic standpoints. The regional acid aspiration, confined only to the right lung, allows the long-term animal survival without any kind of mechanical support. In the acute phase (24 hours after injury) of the ARDS model we found

altered endothelial permeability, massive inflammatory cell infiltration in the alveoli and dysfunction in terms of oxygenation. Interestingly, after two weeks from lung injury we discovered the formation of fibrotic scar and the persistent derangement of lung compliance (index of mechanical properties of lung). This long-term low-mortality model permits the study of treatment effects of different therapeutic strategies on lung injury and repair (57).

2. TREATMENT

No specific therapeutic strategies are now available for ARDS patients in order to reduce the alteration of endothelial-alveolar permeability and the following inflammatory reaction. The only therapeutic approach is the preservation of cellular and physiological functions, such as gas exchange, organ perfusion and aerobic cellular metabolism. The first need is to maintain oxygenation and to remove carbon dioxide, and the standard approach in ARDS patients is mechanical ventilation, that is not a true therapy but a mere support to vital functions. In fact improvement in the supportive care of ARDS patients may have reduced the mortality rate (58, 59). Treatment should take care the underlying cause of ARDS and should pay attention to treat infections (sepsis or pneumonia) (1).

2.1 Non-pharmacological strategies

MECHANICAL VENTILATION. At moment there is no a safe method of mechanical ventilation that assures an adequate gas exchange and, contemporaneously, avoids complications in ARDS patients, because it strictly dependent on the individual. Mechanical ventilation could become dangerous, the so-called ventilation induced lung injury (VILI), and could worsen a pre-existent lung injury.

PRONE POSITIONING. A particular subpopulation of ARDS patients (with severe hypoxemia and severe ARDS) are positively influenced by pronation. Prone position alleviates lung compression and redistributes lung edema to less perfused areas (60).

EXTRACORPOREAL MEMBRANE OXYGENATION (ECMO). ECMO is an extracorporeal technique that provides oxygen support to ARDS patients. Blood from patients passes into an external "lung" membrane an returns to patients. Artificial lung membrane allows an oxygenation and carbon dioxide removal (61).

2.2 Pharmacological strategies

CORTICOSTEROID THERAPY. A great interest has been developed in anti-inflammatory drugs (61). Studies performed using corticosteroids showed controversial results, and for this reason corticosteroids are not routinely used to treat ARDS (61).

INHALED PULMONARY VASODILATOR. Inhaled pulmonary vasodilators, such as nitric oxide (NO), should be useful tools to correct alterations in ventilation/perfusion ratio. But NO did have effects on neither mortality or duration of mechanical ventilation (62).

β_2-AGONISTS. Treatment with β_2-agonists facilitates edema removal and vasodilation and it seems to have also an anti-inflammatory effect. From clinical trials, conflicting results have been obtained: the intravenous administration lead to a reduction of edema (63), whereas the inhalation via (64) did not confirm the promising results.

EXOGENOUS SURFACTANT. Surfactant therapy is routine in neonatal care for the prevention and treatment of infant RDS and other causes of lung injury, since its deficiency is the putative cause of this syndrome (65). As already described above, ARDS is characterized by relative surfactant deficiency,

dysfunction and inhibition, so exogenous surfactant administration seems to be a plausible therapy. Actually treatment with exogenous surfactant demonstrated less efficacy in ARDS than in RDS. Different causes may explain this fail: inadequate pharmaceutical preparations, insufficient dose, wrong administration route and/or time, or the inability to affect the underlying cause of ARDS (65).

Both animal and human studies have been performed to establish the right exogenous surfactant treatment, but conflicting results have been obtained. Most of them suggest that in ARDS induced by direct causes (such as acid aspiration) the response is more positive than in indirect causes.

Animal studies: Multiple studies have been performed with the aim to optimize delivery protocols, doses and timing of therapy (65). Some groups have reported respiratory improvement with surfactant aerosol, other with instillation of surfactant. Lewis et al. (66) have studied different surfactant delivery in a lung-lavaged sheep model, demonstrating various factors that contribute to the pulmonary distribution of exogenous surfactant and its physiologic effectiveness.

In 1998 van Helden and co-workers (67) demonstrated that Curosurf (porcine-derived surfactant) had a therapeutic efficacy in early-stage ARDS in a LPS-induced lung injury rat model. Intratracheal administration of exogenous surfactant (one bolus) improved respiratory frequency and decreased mortality (after 4 weeks), pulmonary edema and inflammatory cells recruitment in alveolar space. In line with this study we have recently found similar results in our unilateral murine model of acid aspiration (68). We showed that an intratracheal single bolus of exogenous surfactant (Curosurf®, Chiesi, Italy)

leads beneficial effects on lung function (respiratory system static compliance) up to two weeks after lung injury induction. To explain the positive effect on lung mechanics we hypothesized a role of exogenous surfactant in modulating inflammatory response, rather than the direct effect of surfactant on lung compliance, since it was observed two weeks after treatment. Histological findings support this hypothesis, in fact we found a significant reduction in terms of chronic inflammatory cells in surfactant-treated mice. Mittal and Sanyal (69) supports the anti-inflammatory properties of exogenous surfactant. In a rat LPS induced lung injury the authors demonstrated that exogenous surfactant (intratracheal) exert anti-inflammatory effects, by reducing the production of cytokines and by down-regulating macrophages and neutrophils infiltration in the lung.

Human studies: Controlled clinical trials on surfactant treatment in ARDS patient have been unsuccessful in adults. Different studies (70-72) have showed principally an improved oxygenation. In some cases the improvement of oxygenation was revealed only in a sub-group of patients with sepsis (73), whereas in the study by Spragg et al. (74) it was not linked to any long-term benefits. On the contrary Anzueto et al. (75) found no oxygenation improvement and no effect on morbidity and mortality, and Kesecioglu et al. (76) reveled even side effects.

3. IMAGING

"Molecular imaging is the visualization, characterization, and measurement of biological processes at the molecular and cellular levels in humans and other living system" (77). Imaging plays important role in the understanding of ARDS pathophysiology and in the development of new treatments for this syndrome (78). It replaces the currently available other biomarkers for lung injury (79). The other biomarkers, that are usually used in clinics, reflect the systemic situation, such as serum analysis, or are invasive, such as bronchoalveolar lavage (BAL) (79). Imaging is surely more sensitive and reproducible and less invasive.

3.1 Computed tomography (CT)

CT is an imaging technique that generates image taking advantage of the different X-rays attenuation properties of tissues (80). A series of equally-spaced projection images are taken around the animal and then are reconstructed with an algorithm to produce 3-dimensional images (81). Each pixel (2-D) or voxel (3D) in the images has a value depending on the density of the tissue, which it belongs to. To better and univocally analyze images a density scale was established. This scale is referred to as CT number or Hounsfield units (HU), which associate each density value to a one grey tone. Value zero is assigned to water, tissue that are less dense than water (like air) are negative (-1000) on the Hounsfield scale, whereas material with higher density (like bone) are positive (+1000). It is possible to perform longitudinal and repeated analysis in a non-destructive manner, enabling comparison with histology (82). In preclinical studies Micro-CT has different kind of applications such as bone study, vascular structures. Of course the use of different kinds of

contrast agent allows to perform CT scans on several organs, such as liver (by using liver-specific contrast agent), kidney and gastrointestinal tract (83).

3.1.1 Lung and CT

The lungs are very suitable for CT imaging, since they have a strong density difference respect to surrounding tissues (84). CT may be a useful tool to evaluate structural and functional aspects from lung parenchyma and the bronchial tree (85). It allows to study lung function in acute and chronic small animal pulmonary disease models (82). The first CT clinical study was performed 1986 (86) when Gattinoni and coworkers observed the morphological density changes correlated with the modifications of positive end expiratory pressure (PEEP). Since then, many studies using CT have been performed aimed at better understanding the pathophysiology of ARDS and at discovering novel successful treatment strategies. Several studies have contributed to study the more protective ventilator strategy, that entails a lower tidal volume (87), the relationship between lung strain (ratio between tidal volume and functional residual capacity) and tidal volume (88) or PEEP (89), and the patient position (prone/supine, 90). In a study in 2010 (91) the surfactant effects on the re-aeration of previously poor-to-nonaerated lung regions was demonstrated. It was demonstrated (92) that CT is useful to describe the ventilation and perfusion of whole lungs of ARDS patients by infusing intravenous contrast agent. CT could provide precise measurements of tissue mass and volume of many human organs (93). Indeed different investigators have measured the end expiratory lung volume (EELV) and the alveolar recruitment through CT imaging (94, 95).

3.2 Positron Emission Tomography (PET)

PET is an imaging technique that allows in vivo assessment of radiolabelled molecules, by detection of emitted radiation from the body (96). It involves the use of a radionuclide, with a short half life. This isotope is bound to a metabolically/biologically active molecule and, after a waiting period (depending on its own properties) while the molecule becomes concentrated in the tissue of interest, the isotope decays by emitting a positron, an antiparticle of electron with opposite charge. The emitted positron covers a short distance (less than 1mm) and immediately combines with an electron, resulting in the annihilation of the two particles. All the mass are converted into electromagnetic radiation, that appears as two 511keV gamma photons at almost 180 degrees to each other. 511keV is equal to the rest mass energy of the electron and the positron (96). The two photons are simultaneously (with difference of almost nanoseconds) detected by a scintillator (coincidence detection technique) and form a light that reaches a photomultiplier. Depending on where the photons are detected by detector, it is possible to know the correct position in the body. Different kind of radionuclides are used for PET imaging, but all of these have a short half life. The most commonly used is fluorine-18 (almost 110 min.), but also carbon-11 (20 min.), nitrogen-13 (10 min.) and oxygen-15 (2 min.). As mentioned above, radionuclides are linked to molecules that are physiologically presented in the body, such as glucose (or its analogs), water and ammonia.

3.2.1 Radiolabelled molecules

[^{18}F]3'-deoxy-3'fluorothymidine (FLT): FLT is a promising PET marker for proliferation (96), since it can be caught by thymidine kinase (TK-1) in the proliferating cancer cells and it remained here.

[^{15}O] radiolabelled water ([^{15}O]H$_2$O): Oxygen-15 radiolabelled water is useful to analyze tissue perfusion, in fact it allows to measure blood flow in vivo. Its uptake is proportional to blood flow, with no physiological effects (96).

N-benzyl-N-methyl-2-[7,8-dihydro-7-(2-(18)F-fluoroethyl)-8-oxo-2-phenyl-9H-purin-9-yl]acetamide ([^{18}F]FEDAC): [^{18}F]FEDAC is a radioligand for translocator protein (TSPO) (98). TSPO is expressed in circulating blood cells, in particular in neutrophils and macrophages and in bronchial and bronchiole epithelium. TSPO expression increased with the severity of inflammation (98).

 [^{11}C]R-PK11195: PK11195 can bind peripheral benzodiazepine-like receptors (97), which are largely expressed by macrophages and it is also known as the mitochondrial 18 kDa translocator protein or TSPO.

[^{18}F]Fluorodeoxyglucose ([^{18}F]FDG): [^{18}F]FDG is the most often imaged molecule with PET. FDG is a glucose analog and, like glucose, interacts with its transporter, which belongs to GLUT family. It can enter the cells and undergoes to glycolysis reaction. In the first step it is subjected to phosphorylation by hexokinases enzymes with the production of [^{18}F]FDG-6-phosphate. Here its glycolytic cycle ends because [^{18}F]FDG-6-phosphate is not the correct substrate of phosphoglucose isomerase and remains in the cells. If it undergoes dephosphorylation, then it will exit the cell, but there are organs (such as lung)

with a low dephosphorylase activity, and in these organs [^{18}F]FDG stays within the cells (99). [^{18}F]FDG is evidently very useful in all cases that are characterized by an intense metabolic activity, with a following intense glucose consumption. In fact [^{18}F]FDG /PET is a standard diagnostic procedure in clinical oncology and it is widely used in neurological and cardiac fields, too (99). PET finds one of its application also in the field of non-tumor dependent inflammation, since inflammatory cells require energy to act, showing so a high cellular metabolic activity. When glucose uptake augments, then significant [^{18}F]FDG uptake occurs, so the increased glucose uptake should be a sensitive marker of inflammation (100).

3.2.2 Quantification of FDG uptake in the lung

The most widely used method of quantifying [^{18}F]FDG in lung is based on standardized uptake value (SUV) (101). The SUV is [^{18}F]FDG uptake in a region of interest (ROI) measured over a certain interval after [^{18}F]FDG administration and normalized to the dose of [^{18}F]FDG injected and to a factor that takes into account distribution throughout the body (such as body weight). SUV equation is:

$$SUV = \frac{AC_{ROI}}{FDG_{dose}/BW}$$

where AC_{ROI} is the average activity concentration in the specified region of interest; FDG_{dose} is the dose of [^{18}F]FDG administered; and BW is the body weight. SUV quantification is affected by many factors, deriving from technical errors or biological/physical factors (102).

- SUV includes both blood and tissue activity in the studied ROI, so the variability in tissue blood volume between subjects could influence the uncertainty of the SUV estimate.

- Increasing blood glucose levels induce lower uptake levels.

- Image artifacts or respiratory motion could affect the SUV quantification.

- SUV outcome is strongly dependent on size and type of used ROI.

Other methods are studied to measure [^{18}F]FDG uptake in the lung in order to avoid the inadequacy of SUV method. The tissue-to-plasma activity ratio is obtained by dividing the tissue activity data during the late imaging frames by the radioactivity in the plasma measured with the mean of two blood samples withdrawn at the end of that frame period (99). Other compartmental models, that use dynamic indices from kinetics of [^{18}F]FDG , were created (99).

A) Two-compartment (Patlak) model: this model entails a central compartment in equilibrium with blood plasma and a peripheral one with the radiotracer trapped in. Patlak plot allows to analyze and identify the pharmacokinetics of the tracer using a linear regression between the [^{18}F]FDG activity in an ROI normalized to plasma activity and the integral of plasma activity in time normalized to plasma activity. The Patlak K_i (net uptake rate) of the studied tissue is the slope of the straight portion of the curve.

B) Three-compartment (Sokoloff) model: it has a blood, a precursor and a metabolic compartment. This model includes the assumption that once phosphorylated, the radiotracer is irreversible trapped in the tissue, but it does not take into consideration that in inflamed lungs there is a further

compartment (edematous tissue) that is separated from cells with [^{18}F]FDG.

C) Four-compartment model: it has been created for injured lung, in which pulmonary edema can increase the distribution volume of [^{18}F]FDG . The fourth compartment refers to an extravascular and noncellular compartment.

3.2.3 Lung and PET

Many studies (103-105) have used PET imaging to quantify inflammation in patients with pneumonia, cystic fibrosis and COPD. Neutrophils are key participants in the development of inflammatory response and when they are activated they augment the glucose consumption until 20-30 times, since they are aerobic glycolysis dependent (99). Some experimental studies have demonstrated that the [^{18}F]FDG uptake during ARDS is the result of the neutrophils alveolar recruitment and their activation state (106-108), that rises the glucose utilization by the cells, demonstrating that [^{18}F]FDG signal is confined to neutrophils (103, 107). In 1994 Jones et al. have proved in two experimental model of ARDS in rabbit that PET imaging is a useful tool for the in vivo measurement of neutrophil activity (107). In particular, the first chronic model was induced by bleomycin administration and is characterized by an intense inflammatory response that progresses towards lung fibrosis; the second acute one was achieved by intrapulmonary instillation of Streptococcus pneumonia (107). A concomitant intravenous injection of tritiated deoxyglucose ([^{3}H]DG) allowed to identify the cell type responsible for the results obtained by PET. Indeed [^{3}H]DG gives the same information provided by [^{18}F]FDG, because it is a glucose analogue, as FDG. In both models they found that [^{18}F]FDG

signal represents the neutrophil activity. Another group (106) have supported these studies demonstrating that PET with [^{18}F]FDG may be a useful tool to study neutrophil kinetics in an oleic acid-induced canine model of ARDS In a sheep model of ventilator-induced lung injury (108), authors found that the number of pulmonary neutrophils correlated with [^{18}F]FDG uptake, confirming the important PET imaging capability and sensitivity to measure the metabolic activation of neutrophils. However they hypothesized that injurious ventilation could promote the metabolic activation also of other type of cells, such as epithelial and endothelial cells, that are responsible for PET signal even with neutrophils depletion. In this respect Zhou et al. (100), in a murine model of ARDS, have observed increased glucose metabolism of lung parenchymal cells, that they hadn't seen in an previous experiment done in dogs. They speculated that there was an apparent species difference, since they found different TBR (tissue-to-blood radioactivity ratio) values between the two experiments. Their hypothesis was also confirmed by neutrophil depletion experiments: even without neutrophil influx in the lung, an increased TBR value was detected, indicating a persisted stimulation of glucose uptake. Overall a growning literature supports further studies about [^{18}F]FDG PET imaging as an indicator of pulmonary inflammatory disease, from diagnosis, to time course monitoring and to evaluation of the effects of anti-inflammatory treatment.

Aim

AIM

ARDS is a life threatening disorder associated to a high mortality and at the moment there is no specific therapy. Different pharmacological strategies have been studied and tested but all of them demonstrated conflicting results. Further studies are necessary to discover a valid treatment for ARDS and preclinical studies are major candidate to develop it. Several studies have been performed using "classical" techniques, such as BAL or histology, but these are post-mortem procedures that entail the sacrifice of the animals. Imaging techniques, in particular CT and PET, enable the in vivo monitoring of lung injury (CT) and inflammation (PET), facilitating also the understanding of the progression of ARDS. Furthermore these techniques are useful in preclinical studies since they represent a non-invasive method to assess novel therapeutic strategies and could be translated to the clinical research setting.

The primary aims of this project were:

1- To verify if PET imaging could be a functional tool to monitor *in vivo* the inflammatory process in our previously described unilateral acid induced lung injury;

2- To evaluate a possible relationship between an early PET signal and late fibrotic evolution;

3- To evaluate the effects of the exogenous surfactant treatment in our murine model of acute respiratory failure.

This project has been made in collaboration with the laboratory of Nuclear Medicine Department and PET Centre, San Raffaele Scientific Institute, Milan, (Dr. Rosa Maria Moresco) which performed PET study and images analysis.

Materials and Methods

MATERIALS and METHODS

1. Animals

All the procedures involving animals and their care were performed in conformity with the relative institutional guidelines which comply with relevant national (no. 116, G.U., suppl. 40, 18/02/1992, no. 8, G.U., 14/07/1994) and international laws and policies (EEC Council Directive 86/609, OJ L 358, 1, Dec 12, 1987; Guide for the Care and Use of Laboratory Animals, US National Research Council, 1996). Animals were maintained under standard laboratory conditions and they had free access to food and water.

2. Experimental design

The whole study was divided into three sets of experiment:

1) Time-course experiment: different animals at different time points were studied.
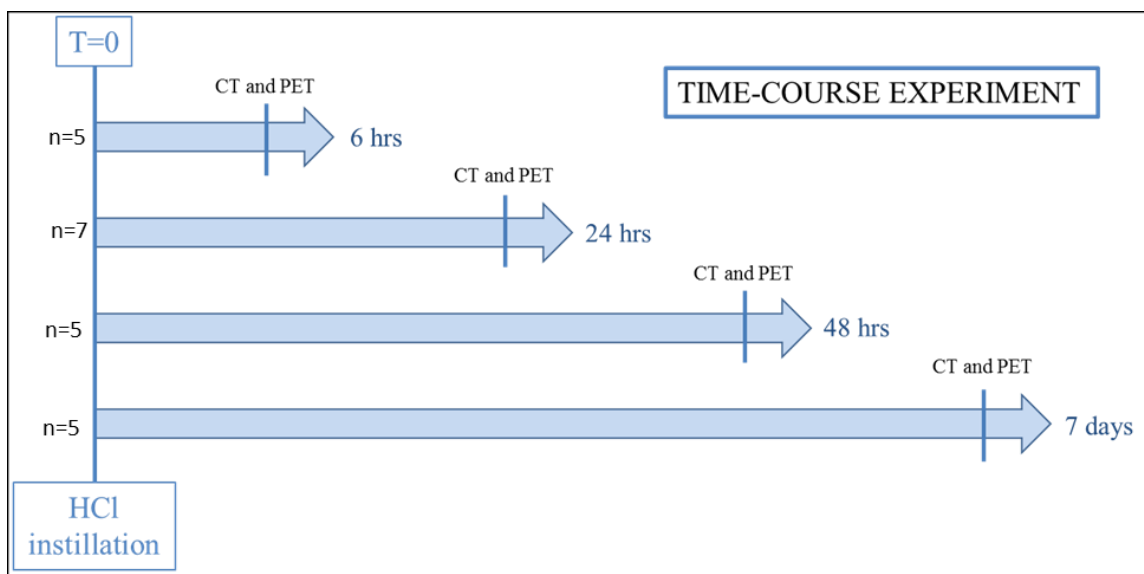
Fig.1 Time-course experiment.

In this first set of experiment we have studied 4 time points (6, 24 and 48 hours and 7 days) after lung injury induction. A further group of mice (n=16) was used to perform broncho-alveolar lavage (BAL) study, in which mice underwent PET scan 24 hours after injury and were sacrificed 48 hours after injury. The aim of this part of experiment was to correlate the imaging (CT and PET) results with histology and bronchoalveolar lavage (BAL) (only for 48 hrs time point). After induction of injury, mice underwent micro-CT and micro-PET scans at the time points reported in figure 1, after which they are sacrificed.

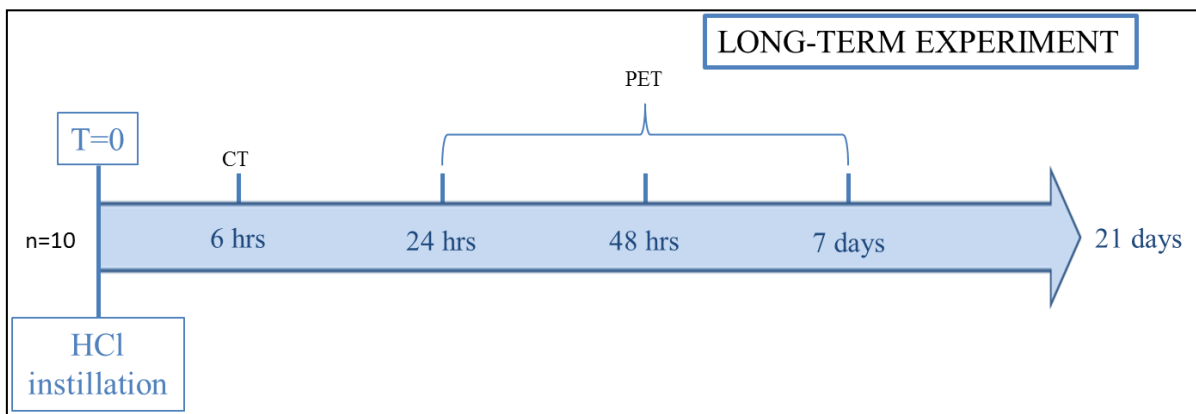2) Long-term experiment: a longitudinal study aimed at studying the fibrotic evolution of injury was performed.

Fig.2 Long-term experiment.

A single group of mice was used in this part of the experiment. Mice underwent micro-CT scan 1 hour after acid instillation and a series of micro-PET scan at the time points studied in the time-course experiment (6, 24 and 48 hours and 7 days). 21 days after acid instillation mice were killed, lung mechanics was measured and lungs sampled for collagen content assay (hydroxyproline assay).

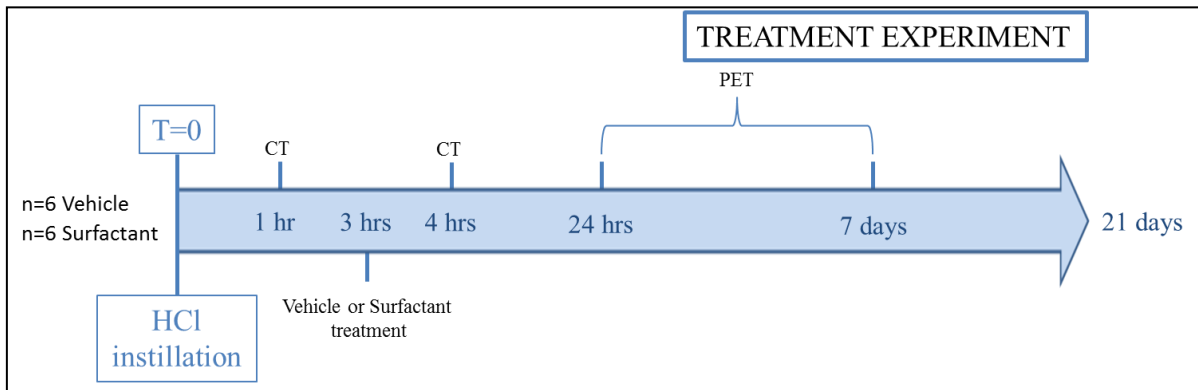3) Treatment experiment: effects of exogenous surfactant treatment were evaluated.

Fig.3 Treatment experiment.

One hour after HCl instillation mice underwent micro-CT scan in order to evaluate the extension and localization (right or left lung) of lung injury before the treatment. Mice received the treatment (Vehicle or Surfactant) three hours after injury and one hour after underwent a second micro-CT scan. 24 hours and 7 days after acid aspiration micro-PET scan was performed on all animals, that were sacrificed 21 days after injury to measure lung mechanical properties and to excise lungs for hydroxyproline content.

3. Induction of injury

Female CD-1 mice (22-28 g, Charles River Laboratories, Lecco, Italy) were used. Mice were anesthetized with an intraperitoneal injection of 400mg/kg tribromoethanol (Sigma-Aldrich, Milano, Italy). Then they were orotracheally intubated with a 22-gauge angiocatheter and mechanically ventilated (Inspira ASV, Harvard Apparatus, Crisel Instruments, Roma, Italy) with these ventilator

parameters: tidal volume 8-10 ml/kg, respiratory rate 130 min^{-1}, positive end-expiratory pressure 2-2.5 cmH$_2$O and fraction of inspired oxygen (FiO$_2$) 1. A small tracheal incision was made and a PE-10 catheter, connected to an Hamilton syringe, was introduced in it a directed towards the right bronchus, facilitated by the anatomy of murine bronchial tree . 1.5 ml/kg hydrochloric acid (HCl) 0.1 M was instilled into the right bronchus through this cannula, while the mouse was continuously ventilated. Once the instillation was performed, the catheter was removed and the tracheal incision was sutured with a 7-0 silk suture thread. Skin was sutured with a 5-0 silk suture thread. During instillation and for the next 10 minutes mice were kept in a reverse Trendelenburg position (45°) and with an inclination of 45° to the right side to confine the instilled fluid to the right lung. Mechanical ventilation was stopped after 10 minutes and mice were extubated as soon as they began to breathe autonomously and then placed in an oxygenated chamber (FiO$_2$ almost 0.5) until full awakening. A group a healthy mice (n=11) was used as control group.

4. Treatment protocol

Three hours after HCl instillation, mice were re-anesthetized with an intraperitoneal injection of 200mg/kg tribromoethanol, orotracheally intubated with a 22-gauge angiocatheter and mechanically ventilated with the same ventilator parameters used in the induction of injury. The tracheostomy was reopened and a PE-10 catheter was again introduced into the right bronchus. 1 ml/kg of Vehicle (sterile NaCl 0.9%) or Surfactant (Curosurf®, Chiesi, Italy) 80mg of phospholipids/ml was instilled. The tracheal incision was re-sutured and mechanical ventilation continued for the next 10 minutes, while animals

were kept in reverse Trendelemburg position. Mice were then extubated and put again in an oxygenated chamber.

5. Imaging procedures

5.1 CT imaging and analysis: Mice were anesthetized (Tribromoethanol, Avertin$^®$ 2.5%, 400mg/kg, ip) and placed prone on the CT table for lung scanning. CT scans were acquired using two MicroCT scanner: a) eXplore Locus (GE Healthcare) with the following parameters: voltage 80 kV, current 450 µA and resolution 93 µm; b) 1176 (Skyscan) with acquisition parameters: voltage 80kV, current 300µA and resolution 35 µm. Images were analyzed using MicroView 2.1 software (GE Healthcare) and CT Analyser (Skyscan). We manually outlined, on each transverse section, the right and left lung's profile separately, excluding main bronchi, heart and vena cava. Based on images obtained with the same procedure in six control (untreated) mice we defined the threshold for hypoaeration as the value of the 95th percentile of the frequency histogram of voxels' densities [corresponding to - 140 Hounsfield Units (HU)]. The weight of each voxel is computed as the product of voxel size and density, which is in turn computed as (CTvox+1000)/1000, where CTvox is the CT number of each voxel expressed in HU. The relative weight of hypoaerated compartments were computed as the sum of the weight of the voxels belonging to each compartment normalized by the sum of the weight of the voxels of the entire lung.
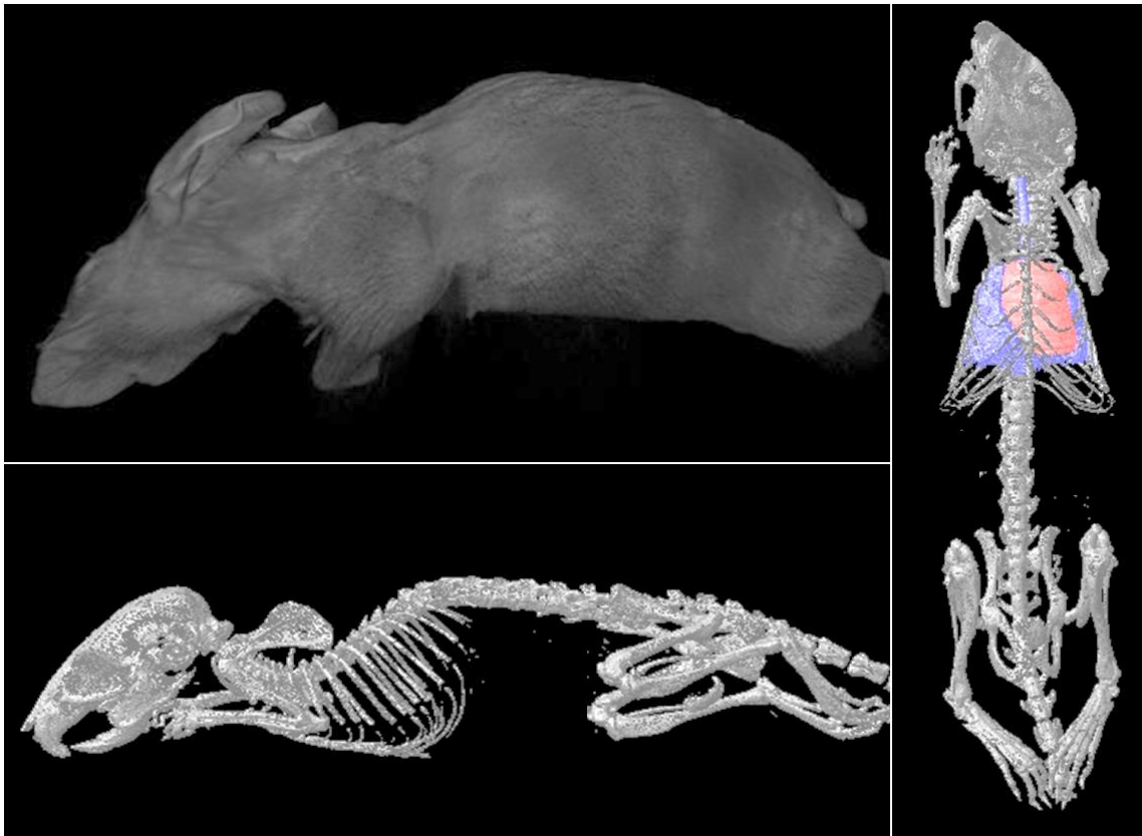
Fig. 3 CT 3D reconstructed scans (healthy mouse). In right panel heart and lungs are outlined.

5.2 PET imaging and analysis: Animals were fasted overnight before PET studies. PET imaging was performed using a YAP-(S)-PET II small animal scanner (ISE, Pisa, Italy) (field of view: 4 x 4 cm; maximum sensitivity: 19 cps/kBq; spatial resolution: 1.8 mm). The [^{18}F]FDG (4.2 ± 0.09 MBq in 50 µl of saline) was administered in the tail vein. 45 min after [^{18}F]FDG administration mice underwent PET scan, whose duration was 30 min (6 frames of 5 min each). For each mouse, we obtained a mean [^{18}F]FDG uptake value, by drawing circular regions of interest (ROIs) in the dorsal area of both lungs, expressed as percentage of injected dose per gram of tissue (%ID/g). These values were calculated by dividing the mean PET-measured values of calibrated radioactivity concentration in tissue (MBq/cc) by the injected doses (MBq) and multiplying by 100. In the long-term study, lung uptake data obtained

43

7 days after injury were expressed as the ratio between right and left lung for the correlation with systemic static compliance (C_{stat}).

5.3 Images analysis: A particular reference system was adopted to place animals in both CT and PET scanners in order to better analyze region of interest in the images. The coordinates of the middle chest were evaluated using CT image. In the Field of View (FOV) we calculated in millimeters the lungs size in z axis and then obtain the organ middle point; this point was centered in the scanner FOV with a laser system pointers. PET and CT images were manually co-registered using PMod 2.7 software. Mean activity for gram of tissue was determined in the injured right lung by drawing Regions Of Interest (ROIs). In order to visualize in the same time co-registered PET and CT images we used Analyze 5.0 software. ROIs (Area=7.49mm^2) were drawn in ten transaxial slices, in the dorsal region of the right damaged lung and on the untreated left lung following the anatomical borders visible in CT image. ROIs include approximately 25 % of the right lung area and 20% of left lung area. The same ROI analysis was conducted also in the control groups to obtain baseline [^{18}F]FDG uptake values.

6. Assessment of injury

<u>Arterial blood gas analysis.</u> Anesthetized mice (Tribromoethanol, Avertin$^®$ 2.5%, 400mg/kg, ip) were orotracheally intubated and mechanically ventilated as described above. After 3 minutes, the chest was opened, the arterial blood (0.5 ml) was sampled from left ventricle and analysed with portable analyzer (i-STAT, Burke & Burke S.p.A.).

Bronchoalveolar lavage (BAL) (only for 48 hrs groups). BAL was obtained in euthanized (via exsanguination) mice in right and left lung separately. In right lung 3 aliquots of 0.6 ml of sterile saline and protease inhibitor cocktail (Complete, Roche) were instilled, withdrawn and stored. In the left lung 3 aliquots of 0.4 ml were used. BAL was centrifuged at 1500 rpm (4°C) for 10 minutes and the cell pellet was resuspended with 0.5 ml PBS (without Ca and Mg) and used for cell counting. Cells were spun with Cytocentrifuge (900 rpm 4°C 5 min) and differential cell analysis by Diff Quik staining (Medion Diagnostic) was performed. Diff Quik staining a commercial Romanowsky stain variant and allows to distinguish cells through morphology analysis. The components are 3 solutions: Diff Quik fixative reagent (methanol); Diff Quik solution I (Xanthene dye) is eosinophilic and dyes cytoplasm; Diff Quik solution II (Thiazine dye) is basophilic and dyes nucleus.

Histology and Immunohistochemical staining. After exsanguination, the lungs were excised, weighted, fixed in 4% formalin for 24 hours (at a pressure of 20 cmH2O for the first 30 minutes), and then paraffin-embedded and sectioned. Hematoxylin and eosin and Sirius red stainings were done on 5μm- and 10μm- thick paraffin-embedded sections to evaluate the lung injury and collagen deposition.

Staining for leukocyte-specific esterase and for macrophages was performed on 5μm-thick paraffin-embedded sections.

Staining for leukocyte-specific esterase, Naphthol AS-D chloroacetate esterase (Sigma Aldrich): slides were incubated in a solution of sodium nitrate, Fast Red Violet BL base solution, TRIZMAL 6.3 buffer, and Naphthol AS-D chloroacetate

solution in deionized water for 3 hours at 37°C. After rinsing, slides were counterstained with Gills hematoxylin solution and coverslipped.

Staining for macrophages was performed with rhodaminated Griffonia simplicifolia Lectin 1 (RL-1102 Vector Laboratories). Stained lung sections were examined microscopically for morphology and positively stained cells. Staining for macrophages was done on 5μm thick paraffin embedded sections. Nuclei were stained with bisbenzimide.

To establish the total number of neutrophils (esterase-positive) or macrophages (Lectin 1-positive) present in the sample, tissue sections were randomly screened (right lung: 10 fields/slide; left lung: 6 fields/slide) at X1000 (0.01mm2/field) and cells were counted. Both results were expressed as number of cells per high-power field (HPF, 0.2mm2). All histological analyses were performed blinded to group assignment.

Lung mechanics: respiratory system static compliance. Lung compliance was measured through pressure-volume curve. Respiratory system PV curves were constructed in euthanized mice (sodium pentobarbital, 200mg/kg, ip) immediately after death in order to minimize post-mortem muscle changes. After a recruitment maneuver (at 30 cmH_2O for 30 seconds), three steps of inspiratory volumes were delivered, starting from functional residual capacity to a total volume of 0.9 ml. For each step, the compliance was calculated as the ratio between the delivered volume and the pressure variation. The three compliance values were averaged (C_{stat}).

Collagen deposition: hydroxiproline assay. To estimate the development of fibrosis, collagen content of lungs was measured using a conventional hydroxyproline method. Lungs were homogenized in 1 ml of PBS, and a 0.5 ml aliquot was hydrolyzed in 6 N HCl at 110°C for 12 hrs. Twenty five microliter aliquots were added to 0. 5 ml of 1.4 % chloramine T (Sigma, St. Louis, MO), 10 % *n*-propanol, and 0.5 M sodium acetate. After 20 min of incubation at room temperature, 0.5 ml of Erlich's solution (1 M *p*-dimethylaminobenzaldehyde [Sigma] in 70 % *n*-propanol, 20% perchloric acid) was added and a 15 min incubation at 65 °C performed. Absorbance was measured at 550 nm and the amount of hydroxyproline was determined against a standard curve.

Statistical analysis. Data are expressed as mean ± S.D. Variables at each time point were compared between left and right lungs by paired t-tests. Correlations between variables were tested by linear regression. P values of less than 0.05 were considered statistically significant. Fisher's r-to-z transformation was performed to establish the significance of the difference between two correlation coefficients. Statistical analyses were performed using by Sigmaplot 11.0 (Systat software Inc.) and SPSS (IBM SPSS Statistics, Version 19.0).

Results

RESULTS

1) TIME-COURSE EXPERIMENT

Pulmonary function: oxygenation. After 6 and 24 hours from acid instillation partial pressure of oxygen (PaO_2) (54±6 and 67±3 mmHg, respectively) was reduced compared to healthy mice (black line in Fig. 4). These results confirm our previous findings (57): monolateral HCl instillation induced a deterioration in gas exchange in the first 24 hours. As expected at 48 hours oxygenation recovered, remaining above 100 mmHg thereafter.
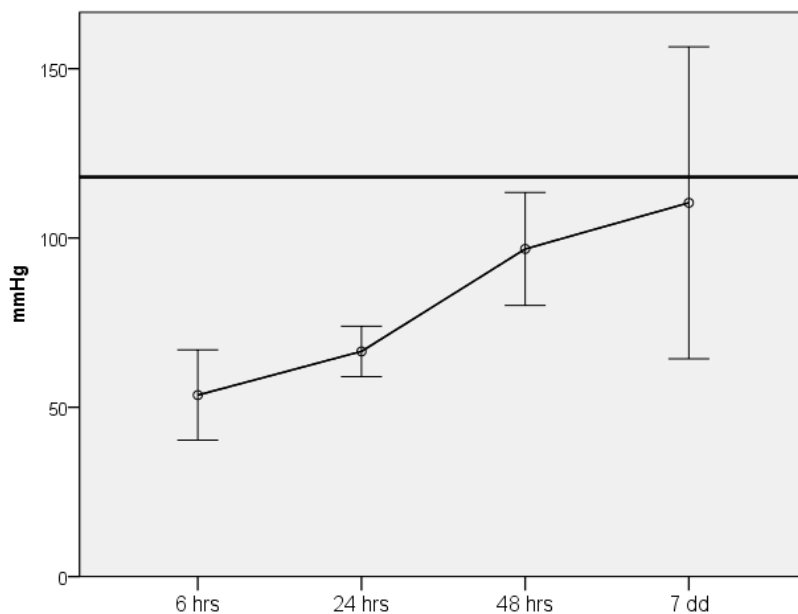

Fig. 4 Gas exchange. Time course of oxygenation after HCl instillation.

Micro-CT imaging. We found an increased percentage of hypoaerated tissue in both lungs 6 hours after injury (31±21 % in right and 29±18 % in left lung). But at 24 and 48 hours, areas of abnormal density were differently ($p < 0.001$) distributed between the right and the left lung. The hypoaeration was partially resolved at 7 days, as shown in figure 5.
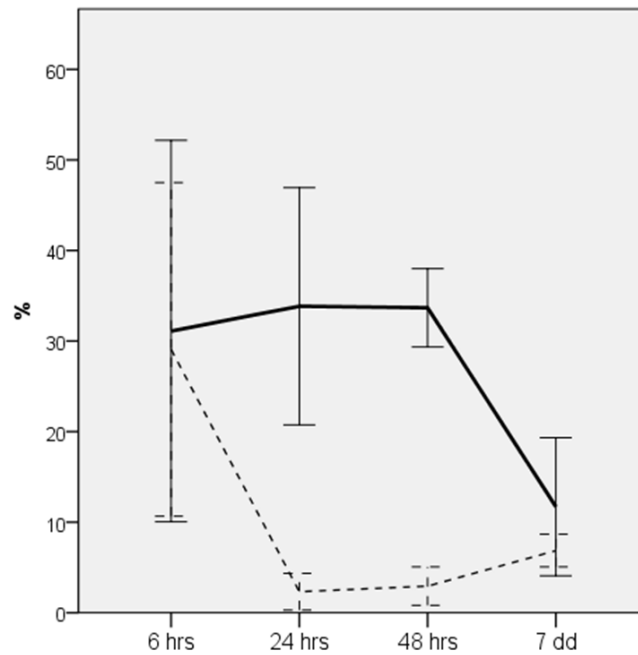
Fig. 5 Percentage of hypoaerated areas in right (solid line) and left (dotted line) lung. Values were expressed as mean ± S.D.

<u>Micro-PET imaging.</u> [^{18}F]FDG uptake (Fig. 6) in the right lung was significantly higher than in the contralateral lung up to 48 hours after injury. PET signal returned to baseline values 7 days after HCl administration (Table 1). At each considered time point [^{18}F]FDG uptake values for both lungs of the injured animals were statistically higher than the values recorded in healthy mice.

	6hrs	24hrs	48hrs	7dd		Baseline (fasting)	Feeding condition
Right lung (n)	2.6 ± 0.3 * § ° (4)	3.5 ± 0.5 * § ° (7)	2.9 ± 0.8 * § ° (4)	1.9 ± 0.2 § (4)		1.4 ± 0.3 (11)	1.6 ± 0.4 (11)
Left lung (n)	1.6 ± 0.3 ** (4)	2.2 ± 0.4 ** (7)	1.5 ± 0.1 ** (4)	1.7 ± 0.1 ** (4)		1.3 ± 0.2 (11)	1.9 ± 0.4 (11)

Table 1. Time course of [^{18}F]FDG uptake (expressed as % ID/g) at each time point in the right and left lungs. *$p<0.05$ compared with contralateral lung; §$p<0.05$ compared with fasting group right lung; °$p<0.05$ compared with feeding group right lung; **$p<0.05$ compared with fasting group left lung; #$p<0.05$ compared with feeding group left lung.

No significant difference in [18F]FDG uptake between right and left lungs was found in the control group, evaluated in fasting condition (Table 1).

Uptake of [18F]FDG was significantly higher in the left lung of HCl-treated mice than in the left lung of control mice studied in fasting condition.
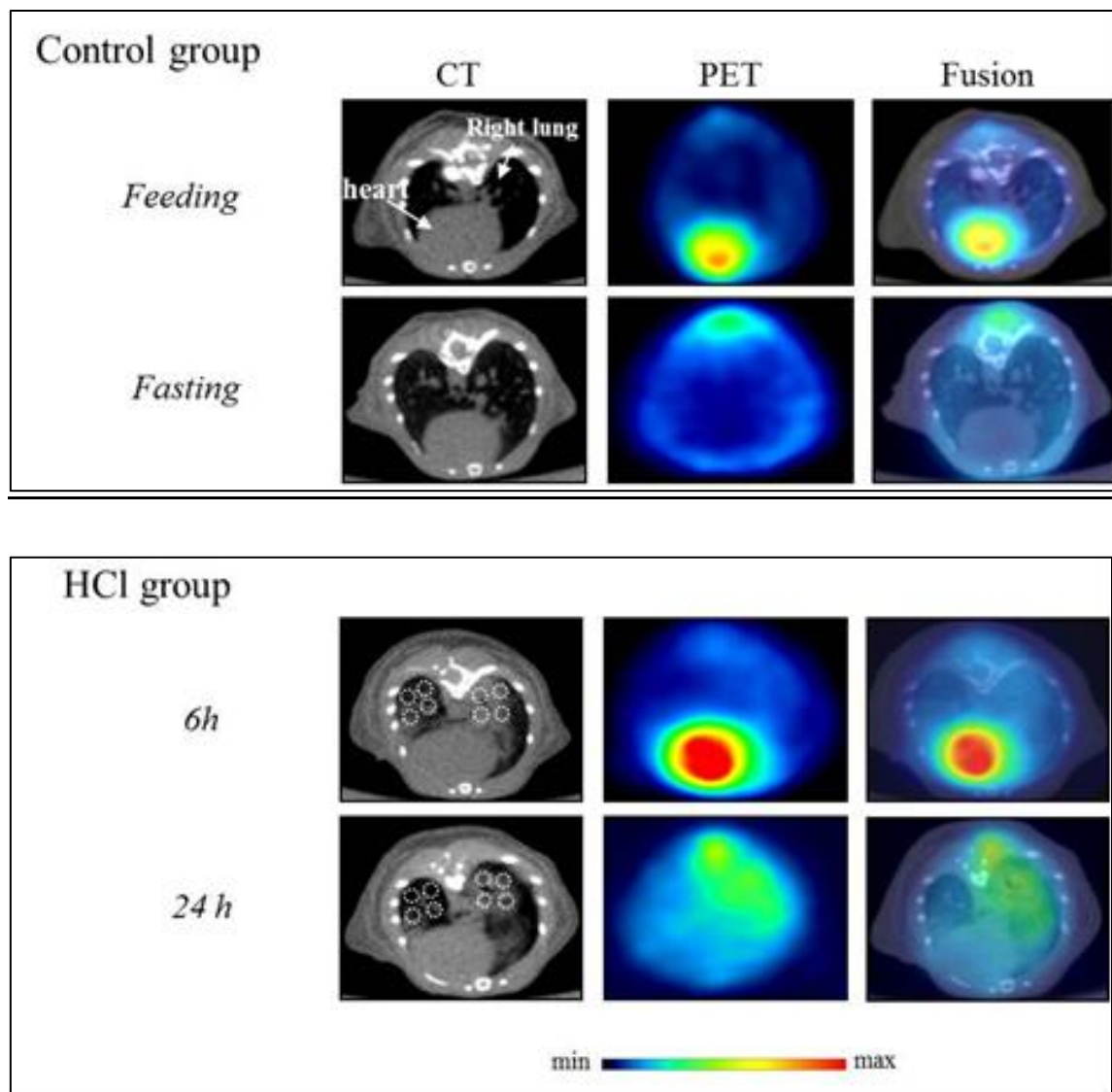

Fig. 6 Control group transaxial images divided into feeding and fasting condition and examples of HCl group images at 6 and 24 hours after acid instillation. In CT images of HCl animals the dashed circles are represent the positions of ROIs in one of the lung slices used for the analysis. © Copyright jointly held by Springer and ESICM 2012.

Correlation CT-PET. [^{18}F]FDG uptake correlated with the amount of hypoaerated tissue in the right lung (R^2 0.24, p=0.03) but not in the left one (Fig. 7).
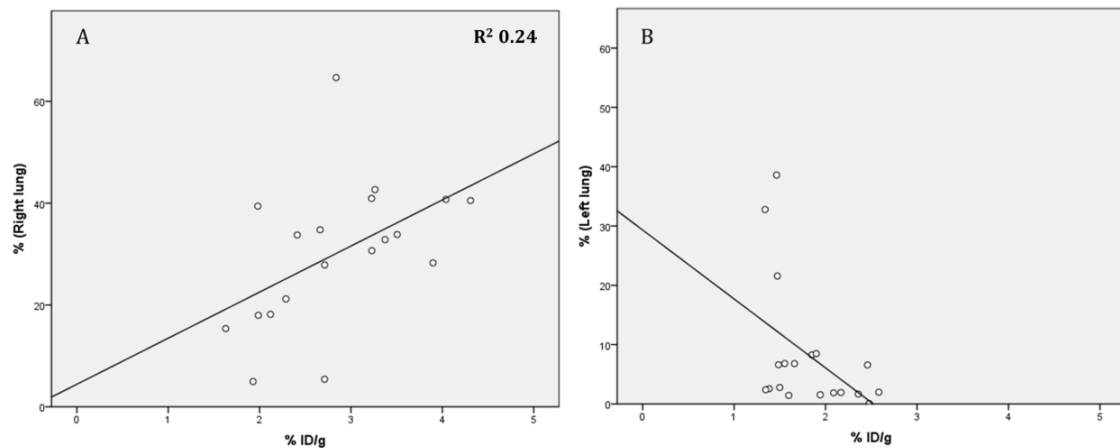

Fig. 7 Correlation between [^{18}F]FDG uptake (expressed as % ID/g) and % of hypoaerated tissue at each time point (6, 24, 48 hours and 7 days) in the right (A) and left (B) lung.

Inflammatory cell accumulation. PMN counts (Fig. 8) differed between the right and left lungs at 24, 48 hours and 7 days (24h: 172±44 vs 86±11; 48h: 50±6 vs 35±4; 7d: 27±5 vs 12±3 per HPF; p<0.05 for all comparisons), while macrophage counts (Fig. 8) differed at 6, 48 hours and 7 days (6h: 83±8 vs 59±10; 48h: 137±10 vs 66±3; 7d: 81±8 vs 54±9 per HPF; p<0.05 for all comparisons).

In both lungs, the time course of the [^{18}F]FDG uptake mirrored (Fig. 9-10) that of the recruitment of PMNs and macrophages, peaking at around 24 hours when PNMs were prevalent. Later, the concentration of PMNs decreased and the [^{18}F]FDG uptake mainly reflected the presence of macrophages.
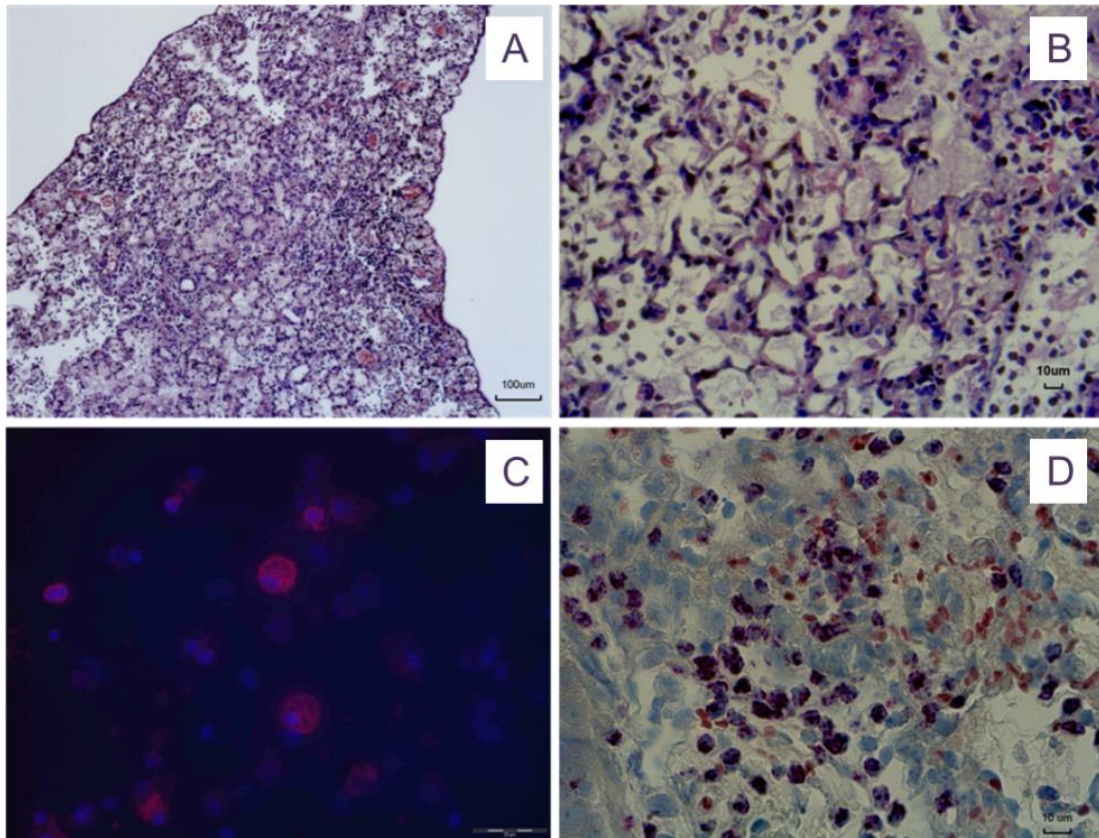
Fig. 8 Histological and immunohistochemical sections. a) and b) hematoxylin and eosin staining (100X and 400X respectively). c.) Lectin 1 staining for macrophages (600X). d) Naphthol staining for neutrophils (600X). © Copyright jointly held by Springer and ESICM 2012.
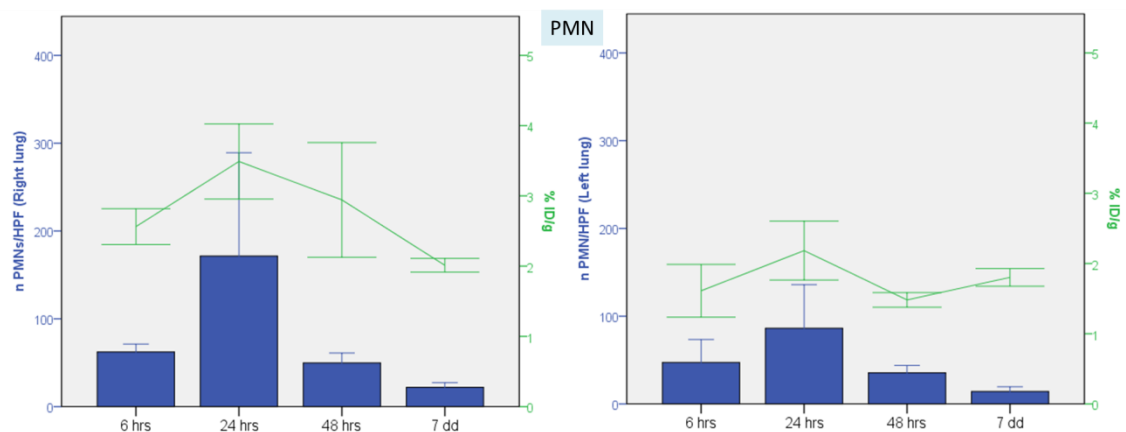

Fig. 9 Time course of neutrophil-specific esterase+ cells (histograms) and PET signal (green line) in right and left lung. PMN counts were expressed n/HPF and [^{18}F]FDG uptake as % ID/g. Values were expressed as mean ± S.D.
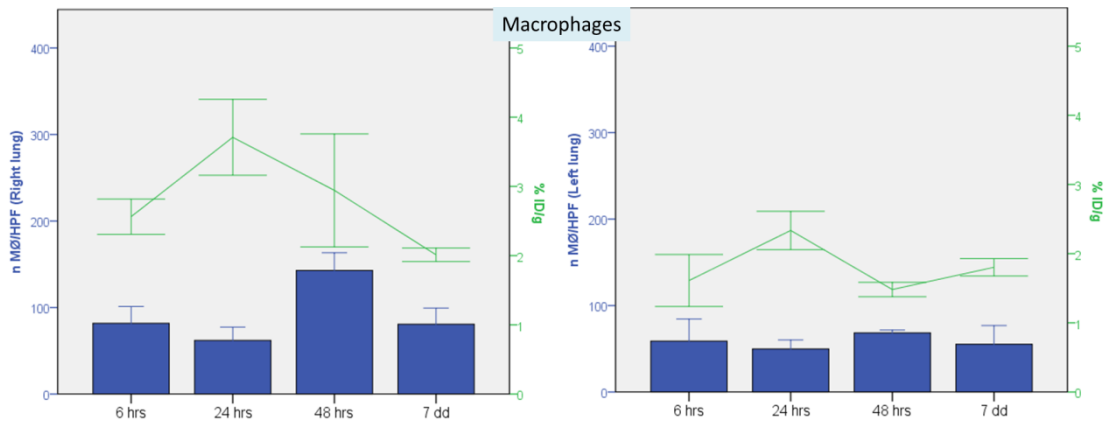
Fig. 10 Time course of macrophages lectin 1-positive cells (histograms) and PET signal (green line) in right lung. Macrophages counts were expressed n/HPF and [^{18}F]FDG uptake as % ID/g. Values were expressed as mean ± S.D.

Correlation inflammatory cells-PET. The PMN count correlated with [^{18}F]FDG uptake both in the right (R^2 0.302, p=0.018) and left lung (R2 0.365, p=0.008). Conversely, the number of macrophages did not correlate with PET [^{18}F]FDG uptake (right lung R^2 0.033; left lung R^2 0.09). However, the correlation coefficients increased (albeit not significantly) if the sum of the two cell types (Fig. 11) was taken into account both in the right (R^2 0.41, p=0.01) and in the left (R^2 0.50, p=0.003) lung (Fig. 12).
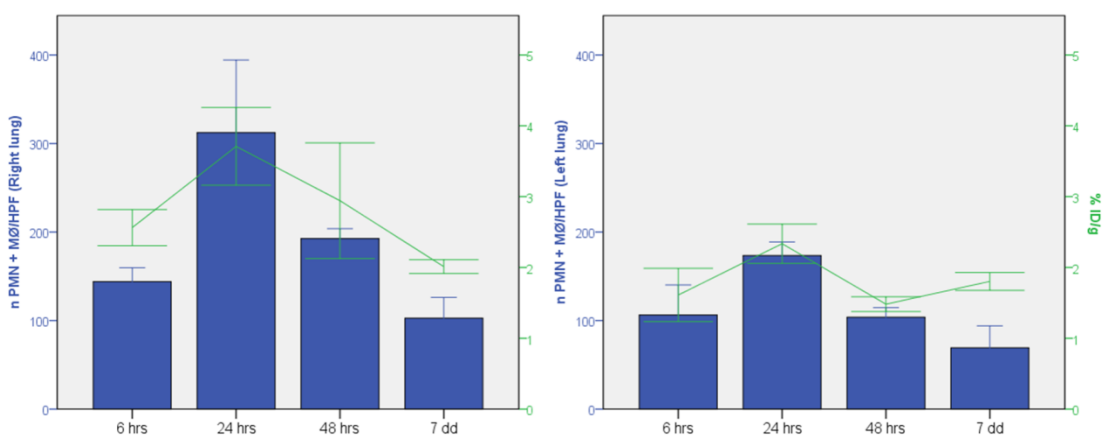

Fig. 11 Time course of the sum of neutrophil-specific esterase+ cells and macrophages lectin 1-positive cells (histograms) and PET signal (green line) in right lung. PMN and macrophages counts were expressed n/HPF and [^{18}F]FDG uptake as % ID/g. Values were expressed as mean ± S.D.
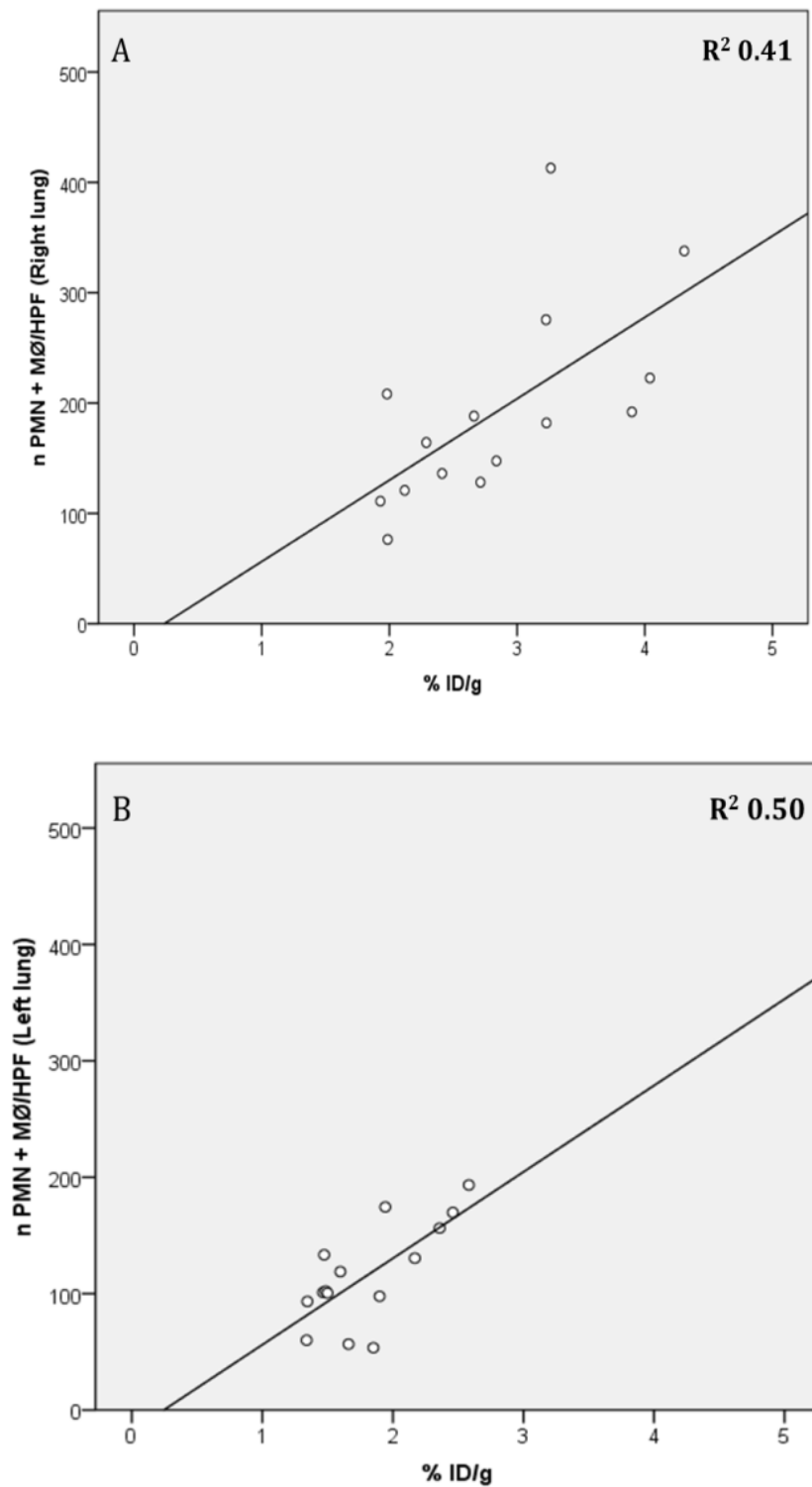
Fig. 12 Correlation between [^{18}F]FDG uptake (expressed as %ID/g) and number of PMN and macrophages on tissue sections (expressed as n/HPF) at 6, 24, 48 hours and at 7 days post-injury in the right (A) and left (B) lung.

Correlation BAL cells – PET. A separate group of animals was sacrificed 48 hours after injury and correlation between recruited cells into alveoli and [18F]FDG signal was evaluated. Total cell count recruited in BAL 48 hours from acid instillation was well correlated (p=0.022) with PET signal measured 1 day before (Fig. 13). If we consider only PMN count the correlation with [18F]FDG signal was maintained (p=0.024, data not shown).
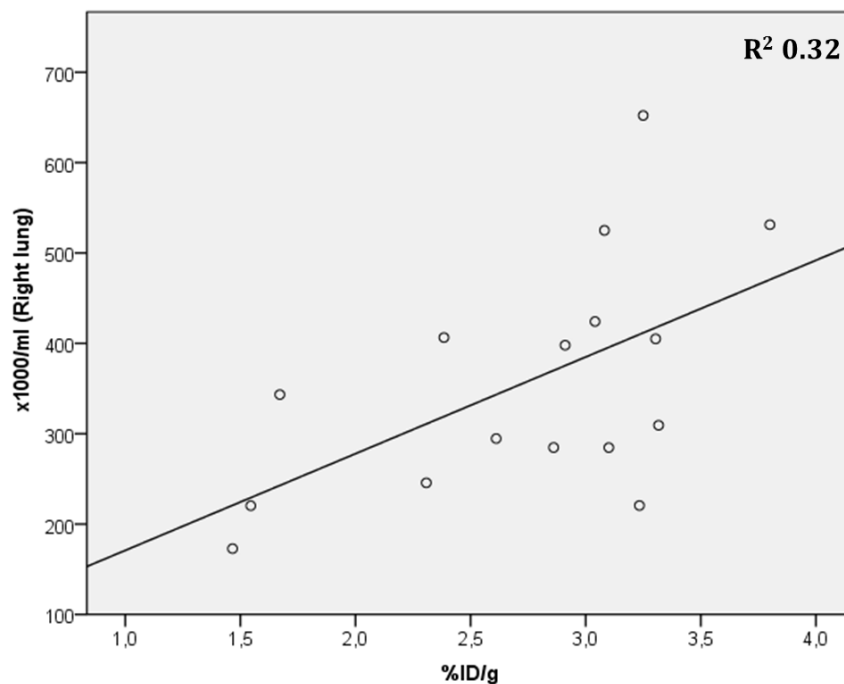

Fig. 13 Correlation between [18F]FDG uptake (expressed as %ID/g) and number of total BAL cells.

Correlation lung function - BAL cells. Figure 14 showed the correlation between the respiratory system static compliance with the number of inflammatory cells recruited in BAL. Indeed it suggests that inflammatory response may influence the pulmonary elastic properties (p=0.003).
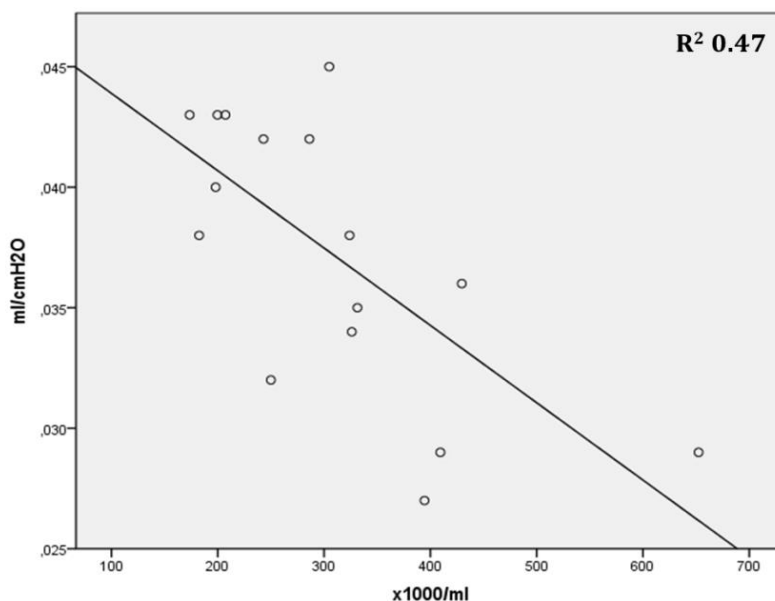
Fig. 14 Correlation between respiratory system static compliance (expressed as ml/cmH$_2$O) and number of total BAL cells.

Correlation lung function – PET. Lung mechanics measured 48 hours after lung injury showed a correlation with PET signal, measured 24 hours before (p=0.02; Fig. 15)
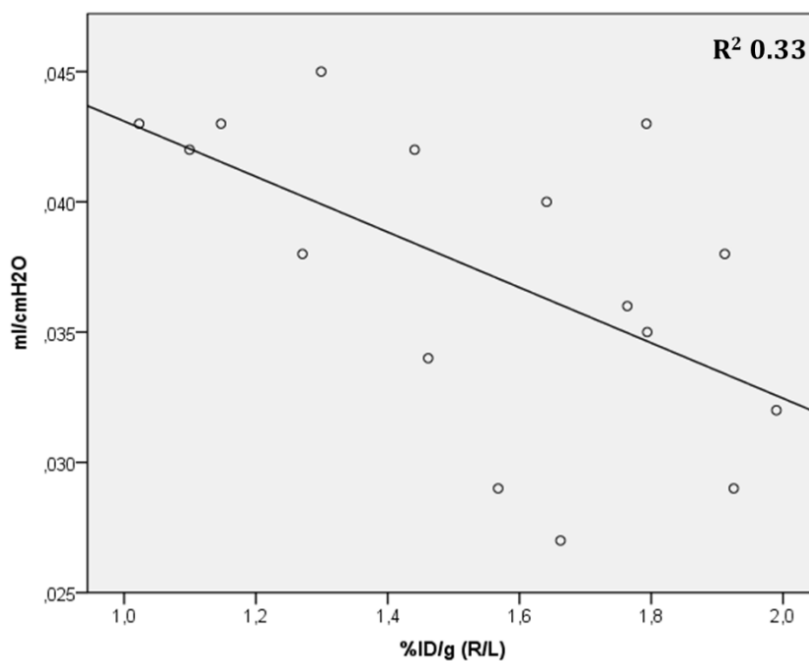

Fig. 15 Correlation between respiratory system static compliance (expressed as ml/cmH$_2$O) and [^{18}F]FDG uptake (expressed as %ID/g).

2) LONG-TERM EXPERIMENT

<u>Pulmonary function: respiratory system static compliance.</u> After 21 days from lung injury alterations in mechanical properties were observed compared to healthy mice (Fig. 16). These results confirm our previous findings (57): monolateral HCl instillation induced a deterioration in pulmonary elastic properties.
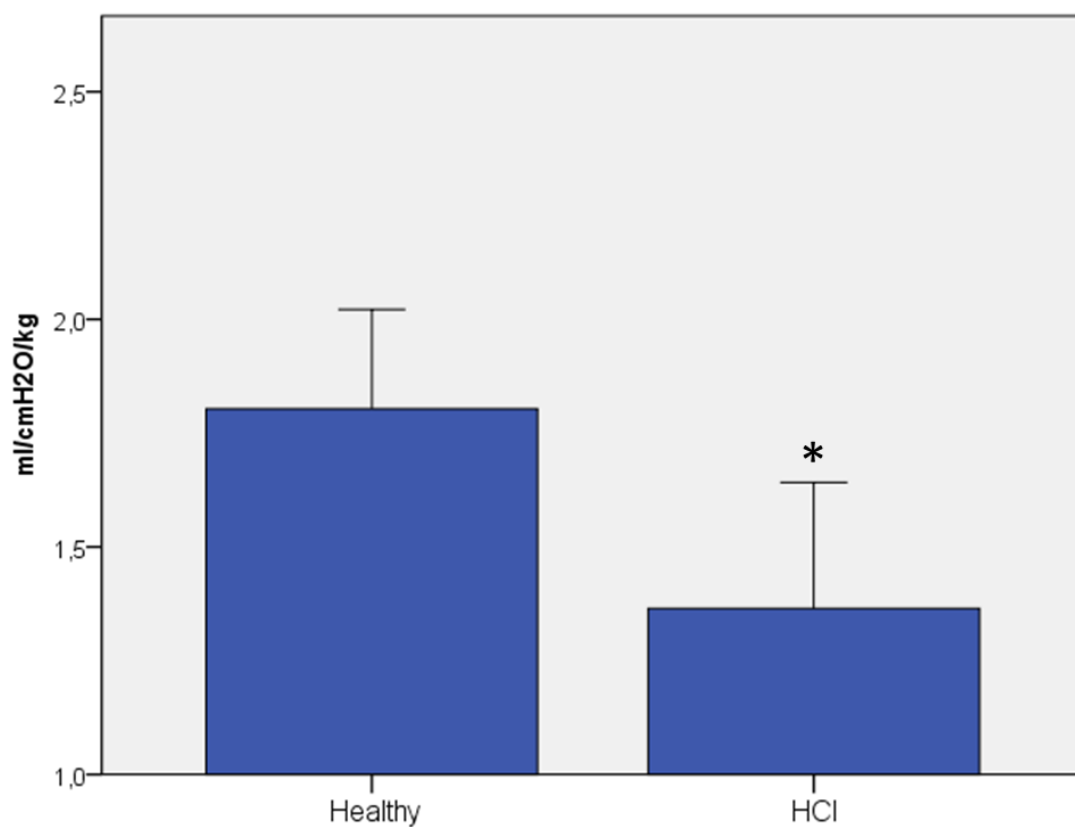

Fig. 16 Respiratory system static compliance measured 21 days after HCl instillation. *p=0.05 vs Healthy mice

<u>Micro-CT imaging.</u> Regions of low aeration, involving 61±19% of the right lung, were observed in all animals on CT scans performed immediately after acid instillation.

Micro-PET imaging. In the right lung of the HCl-treated animals, [^{18}F]FDG uptake (Table 2) was significantly higher than:

- [^{18}F]FDG uptake in the left lung at 6, 24, 48 hours, but not at 7 days post-injury;

- [^{18}F]FDG uptake in the right lung of fed and fasting control mice at each time point.

	6hrs	24hrs	48hrs	7dd	Baseline (fasting)	Feeding condition
Right lung (n)	2.9 ± 0.4 * § ° (10)	2.6 ± 0.4 * § ° (10)	2.5 ± 0.6 * § ° (10)	2.2 ± 0.4 § ° (10)	1.4 ± 0.3 (11)	1.6 ± 0.4 (11)
Left lung (n)	2.3 ± 0.3 ** # (10)	1.9 ± 0.3 ** (10)	2.0 ± 0.4 ** (10)	2.0 ± 0.3 ** (10)	1.3 ± 0.2 (11)	1.9 ± 0.4 (11)

Table 2. Time course of [^{18}F]FDG uptake (expressed as % ID/g) at each time point in the right and left lungs. *p<0.05 compared with contralateral lung; §p<0.05 compared with fasting group right lung; °p<0.05 compared with feeding group right lung; **p<0.05 compared with fasting group left lung; #p<0.05 compared with feeding group left lung.

Correlation lung function-PET. Interestingly, at 21 days, C_{stat} was closely correlated (R^2 0.53, p=0.03) with [^{18}F]FDG levels (expressed as right/left ratio) measured 7 days after injury (Fig. 17).
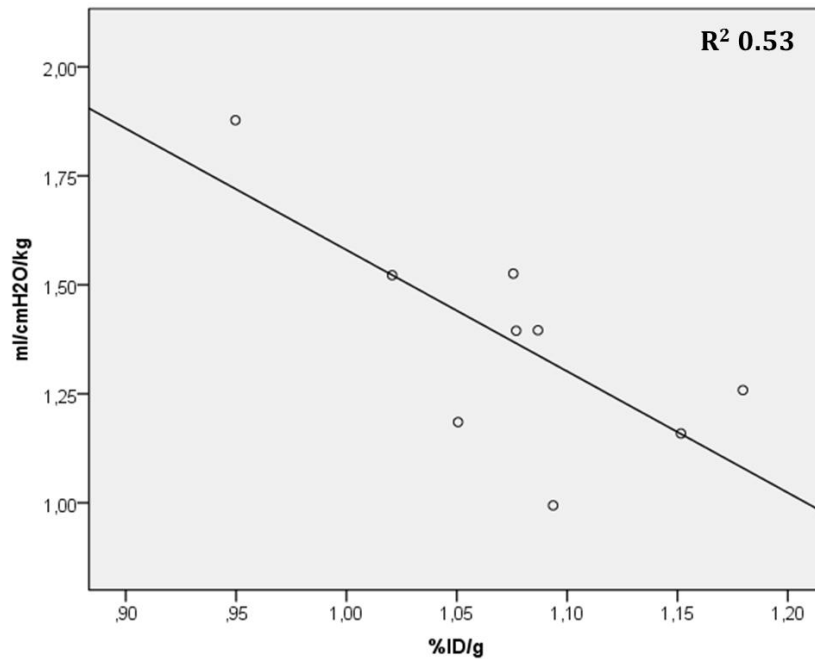
Fig. 17 Relationship between [¹⁸F]FDG uptake (expressed as R/L ratio) at 7 days post-lung injury and respiratory system static compliance after 21 days.

Fibrosis - histology. 21 days after HCl instillation right lung showed marked fibrosing processes with profound loss of normal parenchymal architecture. Alveoli had abundant deposition of collagen fibers and fibroblasts, as shown in histologic sections (Fig.18). Left lung did not show any pathological change.
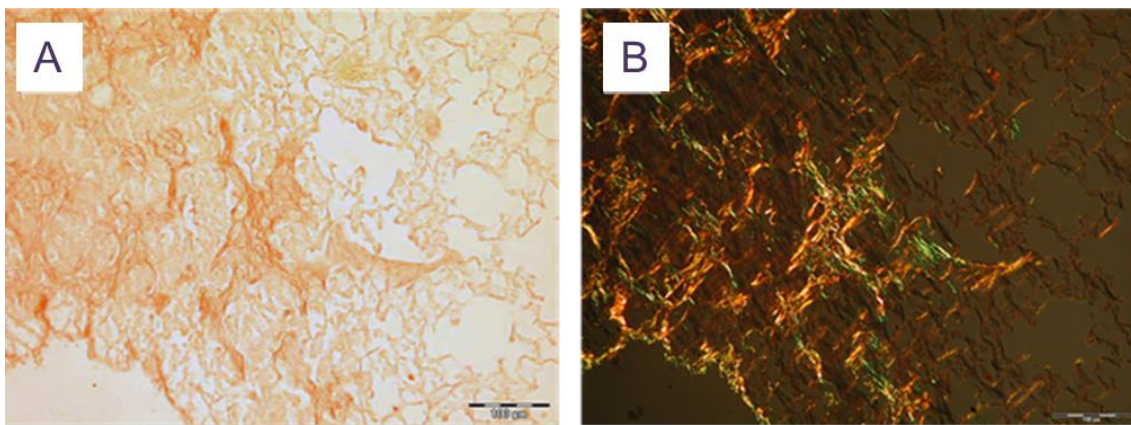

Fig. 18 Collagen deposition: Sirius Red staining (A) and under polarized light (B) (scale bar =100µm) .

<u>Fibrosis – OH-proline content.</u> The OH-proline biochemical assay confirmed the qualitative histological analysis: right lung showed higher collagen deposition (1.46 ± 0.28 µg/mg lung) compared to healthy mice (1.17± 0.14 µg/mg lung).

<u>Correlation fibrosis-PET.</u> The hydroxyproline content in the right lung was closely correlated (R^2 0.55, p=0.01) with PET signal 7 days after lung injury (Fig. 19), while no correlation was found for the left side. No correlations were found between PET signal at the other time points (6, 24 and 48 h) and either C_{stat} or hydroxyproline content after three weeks (p=n.s. for all comparisons, data not shown).

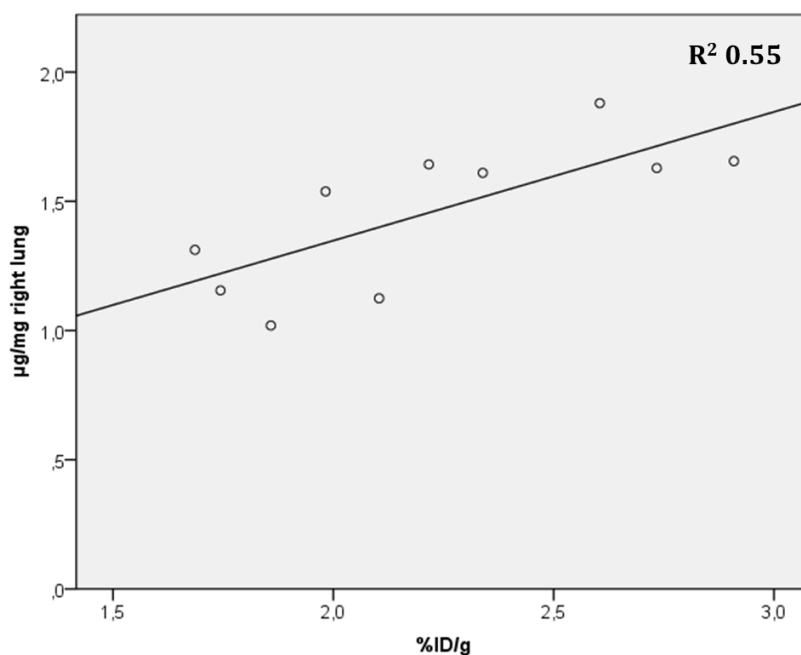**Fig. 19 Relationship between [18F]FDG uptake (expressed as % ID/g) at 7 days post-lung injury and OH-proline content after 21 days in the right lung.**

<u>Myocardium uptake</u>

Since it is well known that myocardial tissue utilizes glucose as nutrient also in feeding condition, we added a group of feed mice, to better understand potential physical artifacts (spillover from heart to lung) on lung radioactivity

concentration measurement, caused by myocardial uptake of radioactivity (109).

As expected, myocardium uptake was present only in fed mice. Visual inspection of the entire set of [^{18}F]FDG PET images derived from injured animals, showed that at 6 hours and 7 days from injury 92% and 78% of mice respectively presented visible radiotracer uptake in the heart. A lower number of mice showed [^{18}F]FDG heart signal at 24 hours and 48 hours after injury (47% and 42% respectively). The loss of significantly difference of [^{18}F]FDG uptake between right and left lung at 7 days in both experimental studies could be due to the heart spillover effect noted at this time point. Indeed, as previously discussed for normal feeding mice, the presence of a spillover effect from myocardium to surrounding lung, cause an overestimation of the level of radioactivity concentration in the left side.

3) TREATMENT EXPERIMENT

<u>Pulmonary function: respiratory system static compliance.</u> After 21 days from lung injury Surfactant treatment has induced a slight improvement in mechanical lung properties if compared to Vehicle group, although not significantly, as reported in Fig. 20.
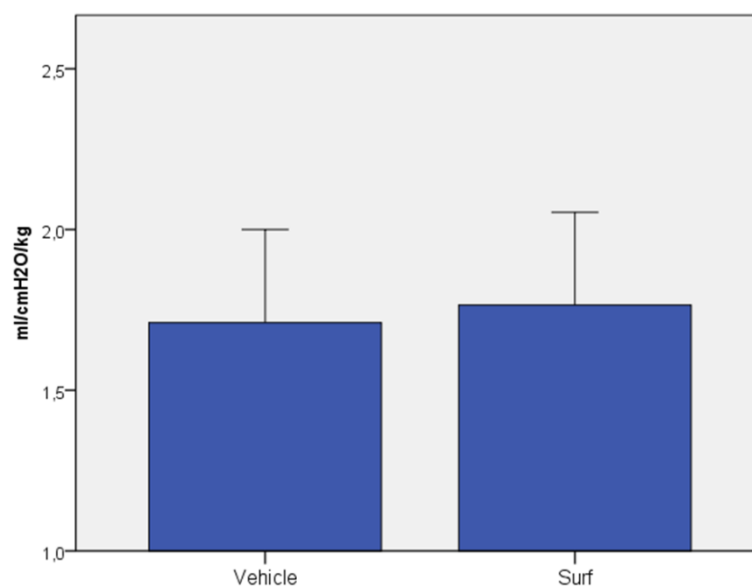
Fig. 20 Respiratory system static compliance measured 21 days after HCl instillation.

<u>Micro-CT imaging.</u> Analysis of CT scans (Fig. 21) performed after HCl instillation and treatment revealed an hypoaeration area in the right lung with extension of 51 ± 27% in Vehicle group and 54 ± 26% in Surfactant group (p=n.s.). Even in left lung there were areas of hypoaeration: 32 ± 32% in Vehicle treated mice and 29 ± 17% Surfactant treated mice (p=n.s.). At the end of experiment all mice showed a reduction in terms of hypoaeration, both in right and left lung: 6 ± 3% (right) e 2 ± 1% (left) in Vehicle group and 7 ± 3% (right) and 3 ± 1% (left) in Surfactant group (p=n.s.).
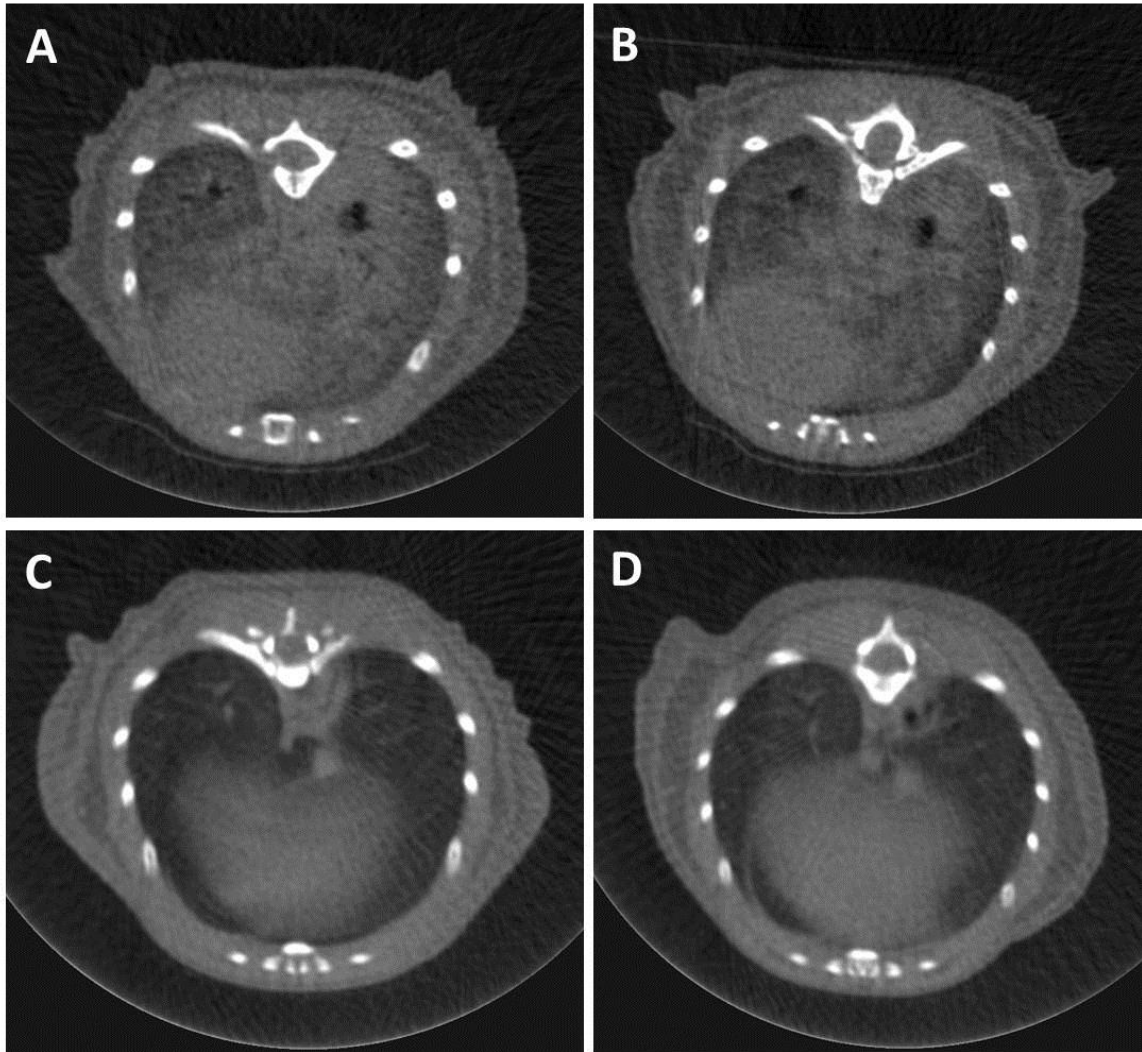
Fig. 21 Examples of CT scans in HCl instilled mice, treated with Vehicle (A, C) or Surfactant (B, D) three hours (above) and 21 days (under) after a lung injury induction.

Micro-PET imaging. [^{18}F]FDG uptake values are reported in table 3. 24 hours after lung injury mice had significantly higher [^{18}F]FDG signal in the right lung compared to the contralateral. After 7 days value of the radioactivity concentration differed no more between right and left lung. No differences were found between Vehicle and Surfactant group.

Time Point	Vehicle			Surfactant		
	Right lung (n=6)	Left lung (n=6)	R/L	Right lung (n=6)	Left lung (n=6)	R/L
24hrs	2.4 ± 0.7*	1.4 ± 0.1	1.5 ± 0.4	2.2 ± 0.6*	1.5 ± 0.3	1.4 ± 0.2
7dd	1.5 ± 0.2	1.4 ± 0.2	1.1 ± 0.1	1.6 ± 0.3	1.5 ± 0.3	1.1 ± 0.1

Table 3. Time course of [^{18}F]FDG uptake (expressed as % ID/g) at 24 hours and 7 days after injury in the right and left lungs. *p<0.05 compared with contralateral lung.

Correlation lung function-PET. Also in this part of experiment we found a close correlation between C_{stat}, measured 21 days after injury, and [^{18}F]FDG levels (expressed as right/left ratio) measured 7 days after injury (Fig. 22), both in Vehicle and Surfactant group (p=0.009).
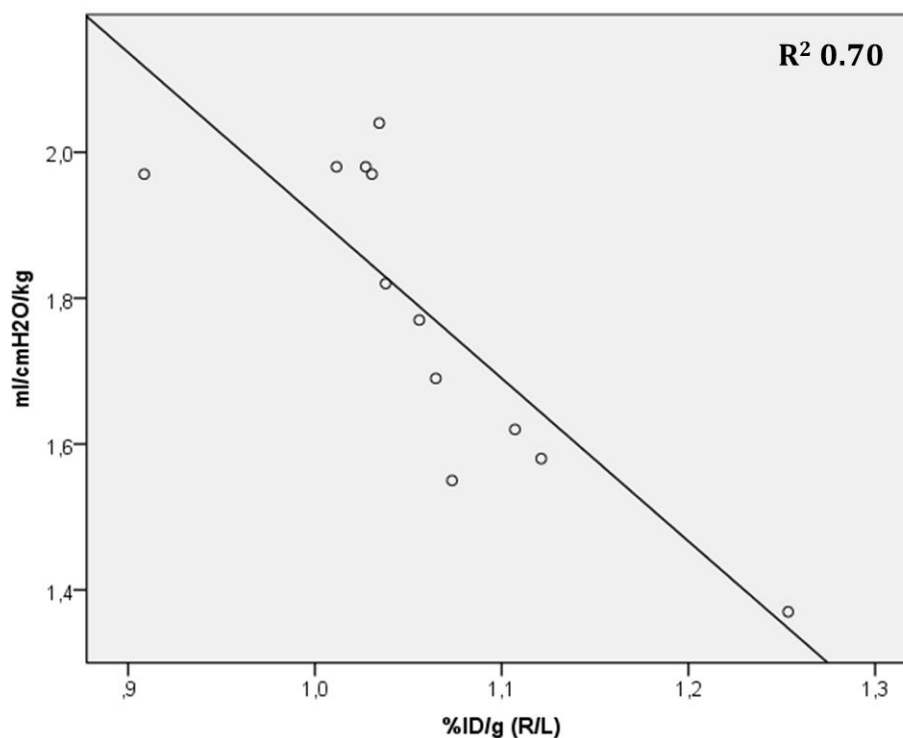
Fig. 22 Relationship between [^{18}F]FDG uptake (expressed as R/L ratio) at 7 days post-lung injury and respiratory system static compliance after 21 days.

Fibrosis: OH-proline content. Surfactant treatment led to a significant reduction in lung collagen deposition. Figure 23 shows OH-proline levels in whole lung: there was a significant difference if compared to Vehicle group.
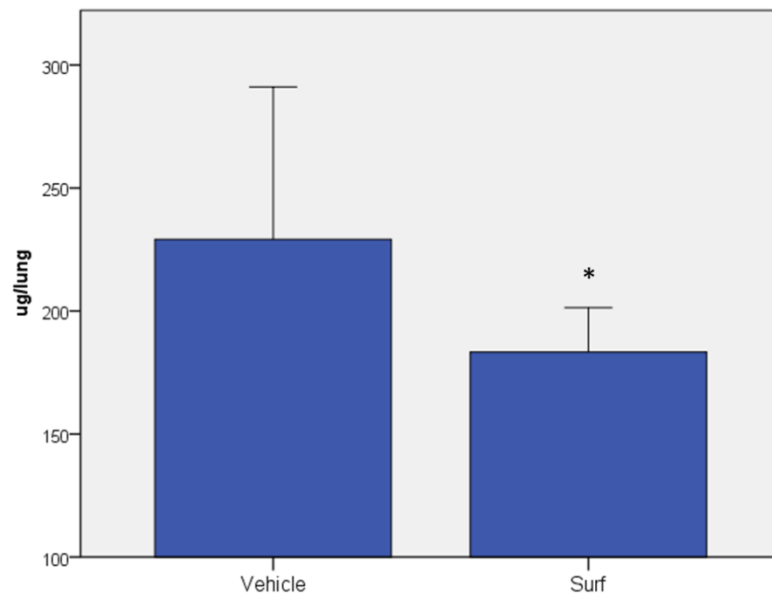
Fig. 23 OH-proline content. *p=0.042 vs Vehicle.

Interestingly the difference between two groups was dependent on the OH-proline deposition in the right lung. Indeed Surfactant treated mice had 115 ± 13 µg, while Vehicle treated mice had 163 ± 61 µg (p=0.026). No differences were found in left lung (Fig. 24).

Fig. 24 OH-proline content in the right and left lung. *p=0.026 vs Vehicle.

Discussion

DISCUSSION

The main purpose of this study was to evaluate the possibility to monitor lung inflammation associated with Acute Respiratory Distress Syndrome using a non-invasive PET imaging technique in a preclinical setting. In particular we aimed at 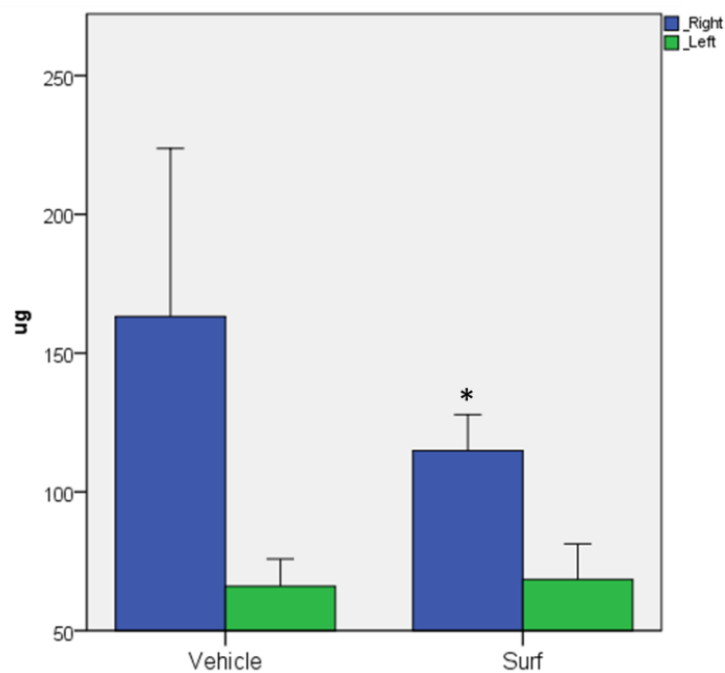characterizing a method for the *in vivo* PET monitoring of lung inflammation in our previously developed experimental (murine) model of ARDS (57) and to match the information obtained from imaging to those obtained from histology and bronchoalveolar lavage, in order to ascertain which cellular types are primarily sustaining the metabolic activity detected by PET. Moreover we sought to disclose the potential relationship between the early inflammatory process occurring in the acute phase and the later fibrotic progression of disease. In the last part of the study we evaluated the therapeutic effects of exogenous surfactant treatment using PET imaging.

It has been reported that the incidence of ARDS is showing a decreasing trend, however its mortality rate is still high, since it remains about 40% (6). An important contributor to its lethality is, at present the lack of any etiological therapy. It is well known that the inflammatory response is initially adaptive, however the persistence or the dysregulation of its activation may lead to serious tissue damage playing a key role in the progression of ARDS. The evidence of a neutrophil-mediated injury in ARDS has been provided by both clinical and preclinical studies and the presence of a marked accumulation of neutrophils during the early phase of the disease has been documented by histological analysis (1). Since neutrophilic recruitment is an important event in the pathophysiology of ARDS, its longitudinal monitoring and quantification might be an useful tool also to evaluate the role played by neutrophils in the progression of the disease and outcome (106). Although neutrophils play

fundamental role in pathogenesis of ARDS, they are not the unique type of cells involved in inflammation. In this process macrophages play a key role as mediator in the recruitment of neutrophils to injury site. Moreover monocytes and neutrophils are directly dependent from each other, and indeed, after monocytes depletion, a decrease in neutrophil recruitment in the lung was revealed (41). Besides their involvement in the early phase of inflammation, macrophages are important cells also in the progression of ARDS.

The availability of a reliable and non-invasive technique for evaluating the inflammatory process during a pathology and for assessing the anti-inflammatory effect of different interventions might enhance the development of novel therapeutic strategies. In this study we have used our model of unilateral acid aspiration lung injury previously published (57).

Time-course experiment - As already observed and described by our laboratory (57), acid instillation induced a severe deterioration of gas exchange, compromising physiological pulmonary function in the first 24 hours (Fig. 4). At 48 hours from lung injury, oxygenation began to recover and PaO_2 remained above 100 mmHg until 7 days. This is the peculiarity of our model, that mimics the clinical ARDS condition, but ensures low mortality, allowing long-term experiments.

Micro-CT analysis of lung injury extension revealed that the first hours of acid instillation were characterized by the presence of hypoaerated areas in the lung involving almost 30% of the whole lung, both right and left. After 24 and 48 hours areas of abnormal density were significantly higher in the right lung compared to the contralateral. These hypoaerated zones are maybe index of the inflammatory process: recruited cells, edema, proteins, necrotic cells and

cellular debris. This concept is confirmed by analysis of the micro-CT and micro-PET scan, that revealed a significant correlation between the percentage of hypoaerated tissue and the inflammatory signal (Fig. 7).

After 1 week, the zone of hypoaeration involved almost 10% of whole lung, with no more difference between the two lungs (Fig. 5).

Regarding the inflammation-related results we showed recruitment of neutrophils and macrophages into the lung, through histological analysis. In particular, their recruitment began 6 hours after injury, but neutrophils count reached their peak at 24 hours and decreased almost to baseline value after 7 days, whereas the number of macrophages peaked at 48 hours, remaining elevated also after 1 week. Our data on neutrophil kinetics are in line with results reported by Reutershan et al. (110), confirming also results present in literature, that describe a massive involvement of neutrophils in the acute phase of inflammation and a persistent presence of macrophages during the late phase (repair or fibrosis). By observing the time course of the [^{18}F]FDG signal we found that it appeared to be more influenced by neutrophils in the first 48 hours, whereas 7 days after it probably depended more on the activity of the macrophages. We hypothesized that both types of cells may contribute to the [^{18}F]FDG signal, since they are both activated and recruited into the lung. Indeed a noteworthy correlation (statistically significant) between [^{18}F]FDG uptake and the number of inflammatory cells recruited into the lung at all the considered time points after injury was seen. We found that the correlation was higher when the sum of PMNs (neutrophils) and macrophages was taken into account as opposed to the single cell types. Even though previous *in vitro* cell studies have demonstrated that monocytes and macrophages cannot increase their glucose uptake to the same extent as neutrophils can (111), other authors,

in *in vivo* (PET) and *ex vivo* (autoradiography) studies, have demonstrated that FDG is taken up by macrophages (particularly if activated) in different inflammatory diseases and malignancies (112). Results obtained by Jones et al. in 1994 (107) are consistent with our results after 24 and 48 hours, and they demonstrated, in a different model of lung inflammation, that [^{18}F]FDG-PET may be used as an *in vivo* index of neutrophil recruitment. In the later phase, we found that PET signal persisted in the lungs 7 days after injury, even though markedly reduced in comparison with the [^{18}F]FDG uptake at 24 hours. A group of mice was assigned to bronchoalveolar lavage (BAL) analysis. As shown in figure 13, the concentration of total cells (neutrophils and macrophages) recruited into alveoli 48 hours after lung injury showed a good correlation with [^{18}F]FDG uptake detected 24 hours before, even if it was weaker than the correlation between histological analysis and PET signal. Indeed histological data includes both alveolar and tissue cells, as PET data does. These results demonstrated, as expected, that the signal detected with PET depends on both alveolar and tissue compartment. In this set of experiment we evaluated also the relationship between the inflammatory process (both BAL cells and PET analysis) and pulmonary function, measuring lung elastic properties (respiratory system static compliance, C_{stat}). Both results (Fig. 14 and 15) demonstrated that inflammation, constituted by cells, proteins and edema, compromise physiologic lung function.

Long-term experiment – A study (113) demonstrated that persistence of the [^{18}F]FDG uptake is associated with scarring of lung tissue. Our unilateral acid aspiration murine model allowed us to study the fibrotic evolution of injury. In fact, as described by Amigoni et al. (57), HCl instillation in the right lung led to a

marked chronic inflammatory and fibrosing processes, obtained by histological and CT analysis. Similarly, in our study, we found a decreased respiratory system static compliance (Fig. 16) compared to healthy mice, probably due to the fibrotic evolution of injury, as demonstrated by Sirius staining and dosage of collagen deposition (hydroxyproline assay). PET signal measured at 7 days showed a correlation with C_{stat} and with collagen deposition measured at 21 days post-injury. These data support the hypothesis that persistent inflammation in the lungs could lead to a fibrotic evolution of the injury.

Micro-CT and micro-PET analysis – As described above we found a good correlation between CT and PET data in the right lung. As expected, areas detected as non- or poorly-aerated by CT scan are also rich in inflammatory activated cells (PET signal). This correlation was not found in the left lung. This result is in line with human data showing increased [^{18}F]FDG uptake also in normally aerated areas (114). The left lung in our murine model is not directly injured by acid instillation, but we demonstrated (57) that the unilateral HCl administration produces an important neutrophilic infiltration (shown by myeloperoxidase activity and histologic analysis) in both lungs.

However, the spillover effect from myocardial [^{18}F]FDG uptake needs to be considered as regard left lung results. Sometimes there was an intense myocardial uptake, that led inevitably to an overestimation of the radioactivity in the areas surrounding the heart, including the left lung. Hypoxic vasoconstriction caused acute pulmonary hypertension and increased right systolic pressure, that could induce myocardial cells to shift their metabolism from fatty acid to glucose oxidation (115), resulting in an increase on [^{18}F]FDG uptake. However, concerning our here presented results, 6 hours after injury,

when most of the animals displayed myocardial uptake, the left lungs had reached levels significantly higher than those observed in the feeding condition, indicating the presence of measurable levels of lung inflammation also in the left lung, as further supported by the significant correlation between cellular infiltration and [^{18}F]FDG uptake. In accordance with previous lung inflammation models, we observed an increased [^{18}F]FDG uptake in the myocardium particularly evident at 6 hours, and 7 days after HCl instillation. However, further studies are needed to clarify the molecular and functional bases of this shift.

Limitations of the study.- We did not analyze PET data using a full quantitative method (e.g. Patlak's plot), since we did not cannulate vessels, in order to make the method simple and non-invasive. We did not directly verify the cell type responsible for the PET signal, either performing microautoradiography with tritiated deoxyglucose ([^{3}H]-DG) (106, 107, 113) or with [^{18}F]FDG, and neither did we used [^{11}C]R-PK11195 for selective imaging of macrophages (116). Moreover, we did not perform PET scans at 21 days, and therefore cannot exclude that further information might have been obtained at this later time point, even though at 7 days the PET signal was already very low.

Advantages – PET imaging, despite a limited sensitivity, may be used to assess the intensity of inflammation, offering two main advantages: the lack of invasiveness allows the application in longitudinal studies performed in the same experimental subject; second, imaging procedure could be translated to the clinical research setting.

<u>Treatment experiment</u> - In the first two parts of the study we have characterized an *in vivo* imaging method to monitor the inflammatory process in our murine model of ARDS. In the last third part we evaluated the effect of exogenous surfactant treatment using CT and PET imaging. As mentioned in the introduction we have recently published (68) one study concerning the effects of a single bolus of exogenous surfactant in the unilateral acid instillation experimental model in the acute (24 hours) and late (2 weeks) phase. In our previous study we have tested (68) two doses of porcine-derived surfactant (Curosurf ®), 40mg and 80mg of phospholipids/ml, but the lower dose showed no effect. On the contrary with the higher dose we found improved arterial oxygen tension (PaO_2) and reduced neutrophil fraction in BAL in the early phase of ARDS (24 hours). Interestingly a single treatment with exogenous surfactant showed beneficial effect also in later phase in terms of static compliance of the respiratory system and chronic inflammation revealed with histological analysis. In light with these results we speculated that exogenous surfactant could reduce inflammatory process, improving lung function.

In this study we used the higher dose of exogenous surfactant (80 mg of phospholipids/ml) and we found a slight reduction (not significant) of PET signal in the right lung in Surfactant treated mice 24 hours after lung injury compared to Vehicle group. Both groups presented, after 24 hours, significantly higher [^{18}F]FDG uptake in the right lung (directly injured by acid) compared to contralateral. Similarly, Surfactant treatment induced a mild improvement in pulmonary elastic properties: figure 20 shows the little difference between groups. The correlation between pulmonary function measured at the end of experiment and PET results obtained 2 weeks before showed a good relationship, confirming results reached in Long-term experiment. The persistent

chronic inflammation is related to a worsening of pulmonary mechanics. Regarding to fibrosis, the dosage of collagen deposition (hydroxyproline assay) revealed that Surfactant administration led to a significant reduction of pulmonary fibrosis. Probably the extension of the fibrotic area is not sufficient to influence the compliance of the whole respiratory system, since it is usually confined only to a lobe of the right lung.

The results concerning compliance and PET imaging seem to be influenced by the reduced number of studied mice. Indeed the absolute values of respiratory static compliance measured here are in line with those observed in our previous study (68). The statistical significance may be reached by increasing the number of mice. Another important point to analyze is the group chosen as comparison, Vehicle group. As already done previously (68), we have decided to instill the vehicle (sterile saline, 0.9%) into a group of mice, in order to subject all mice to an instillation in the lung of a certain volume, as done for Surfactant group. Indeed we thought that receiving a volume of fluid into the trachea, could be injurious per se. This is probably correct, but, at the same time the administration of NaCl in the same area of HCl instillation could dilute acid, by reducing its caustic action. In fact by comparing static compliance in mice from "long-term experiment" and from "treatment experiment" we found a significant difference between mice that received only HCl instillation (1.37 ± 0.26 ml/cmH$_2$O/kg) and mice treated also with vehicle (1.71 ± 0.71 ml/cmH$_2$O/kg).

Conclusion

In conclusion, we have demonstrated that it is possible to measure the inflammatory response in a murine model of acid aspiration lung injury through the use of PET imaging. PET imaging is a powerful tool that is able to provide "real time" evaluation of inflammation. Preclinical FDG-PET imaging allowed, non-invasively, a periodic monitoring of the inflammatory response during ARDS. In our experimental model we demonstrated that not only neutrophils are responsible for cellular activity, but different cell type contribute to $[^{18}F]FDG$ uptake: neutrophils and macrophages are both involved in inflammation development. Our findings show that the persistence of the $[^{18}F]FDG$ signal after the acute phase is associated with an alteration of the lung compliance measured two weeks later, possibly attributable to the fibrotic evolution of injury promoted by the inflammatory infiltrate. Thus, it is possible, in our opinion, that acute treatments of the inflammation capable of reducing the fibroproliferative process, could be monitored using the FDG-PET method. Whit this hypothesis we tested the therapeutical effect of exogenous surfactant administration in acid induced lung injury. We observed a significant reduction of pulmonary collagen deposition, and a relationship between the persistent PET signal and the reduced respiratory system compliance.

Considering our treatment study on exogenous surfactant we speculate that it is possible that acute treatments of the inflammation capable of reducing the fibroproliferative process, could be monitored using the FDG-PET method.

REFERENCES

1- Ware L.B. and Matthay M.A. The acute respiratory distress syndrome. N Engl J Med. 2000; 342: 1334-49.

2- Ashbaugh D.G. et al. Acute respiratory distress in adults. Lancet. 1967; 2: 319-23.

3- Bernard G.R. et al. Report of the American-European consensus reference on ARDS: definitions, mechanisms, relevant outcomes an clinical trial coordination. The Consensus Committee. Intensive Care Med. 1994; 20: 225-32.

4- The ARDS Definition Task Force. Acute respiratory distress syndrome: the Berlin definition. JAMA. 2012; 307: 2526-33.

5- Esteban A. et al. Evolution of mechanical ventilation in response to clinical research. Am J Respir Crit Care Med. 2008; 177: 170-7.

6- Rubenfeld G.D. et al. Incidence and outcomes of acute lung injury. N Engl J Med. 2005; 353: 1685-93.

7- Goss C.H. et al. ARDS Network. Incidence of acute lung injury in the United States. Crit Care Med. 2003; 31: 1607-11.

8- The Acute Respiratory Distress Syndrome Network.Ventilation with lower tidal volume as compared with traditional tidal volumes for acute lung injury and the acute respiratory distress syndrome.. N Engl J Med. 2000; 342: 1301-8.

9- Li G. et al. Eight-year trend of acute respiratory distress syndrome: a population-based study in Olmsted County, Minnesota. Am J Respir Crit Care Med. 2011; 183: 59-66.

10- Thomashefski J.F. Pulmonary pathology of the adult respiratory distress syndrome. Clin Chest Med. 1990; 11: 593-619

11- Matthay M.A. and Zemans R.L. The acute respiratory distress syndrome: pathogenesis and treatment. Annu Rev Pathol. 2011; 6: 147-63.

12- Brower R.G. et al. Higher versus lower positive end-expiratory pressures in patients with the acute respiratory distress syndrome. N Engl J Med. 2004; 35: 327-36.

13- Mercat A. et al. Positive end-expiratory pressure setting in adults with acute lung injury and acute respiratory distress syndrome: a randomized controlled trial. JAMA. 2008; 299: 646-55.

14- Singh N.R.P. et al. Acute lung injury results from failure of neutrophil de-priming: a new hypothesis. Eur J Clin Invest. 2012; 42: 1342-9.

15- Shenkar R. et al. Mechanisms of lung neutrophil activation after hemorrhage or endotoxemia: roles of reactive oxygen intermediates, NF-kB, and cyclic AMP response element binding protein. J Immunol. 1999; 163: 954-62.

16- Grommes J and Soehnlein O. Contribution of neutrophils to acute lung injury. Mol Med. 2011; 17: 293-307.

17- Laffon M. et al. α-adrenergic blockade restores normal fluid transport capacity of alveolar epithelium after hemorrhagic shock. Am J Physiol. 1999; 277: L760-L768.

18- Abraham E. Neutrophils and acute lung injury. Crit Care Med. 2003; 31: S195-S199.

19- Abraham E. Effects of endogenous and exogenous catecholamines on LPS-induced neutrophil trafficking and activation. Am J Physiol. 199; 276: L1-L8.

20- Ognibene F.P. et al. Adult respiratory distress syndrome in patients with severe neutropenia. N Engl J Med. 1986; 315: 547-51.

21- Lee W.L. and Downey G.P. Neutrophil activation and acute lung injury. Curr Opin Crit Care. 2001; 7: 1-7.

22- Azoulay E. et al. Deterioration of previous acute lung injury during neutropenia recovery. Crit Care Med. 2002; 30: 781-86.

23- Matthay M.A. et al. Elevated concentrations of leukotriene D4 in pulmonary edema fluid of patients with the adult respiratory distress syndrome. J Clin Immunol. 1984; 4: 479-83.

24- Parsons P.E. et al. Chemotactic activity in bronchoalveolar lavage fluid from patients with adult respiratory distress syndrome. Am Rev Respir Dis. 1985; 132: 490-3.

25- Steinberg K.P. et al. Evolution of bronchoalveolar cell populations in the adult respiratory distress syndrome. Am J Respir Crit Care Med. 1994; 150: 113-22.

26- Thommasen H.V. et al. Transient leucopenia associated with adult respiratory distress syndrome. Lancet. 1984; 1: 809-12.

27- Kunkel S.L. et al. Interleukin-8 (IL-8): the major neutrophil chemotactic factor in the lung. Exp Lung Res. 1991; 17: 17-23.

28- You A. et al. Stimulation and priming of human neutrophils by interleukin-8: cooperation with tumor necrosis factor and colony-stimulating factors. Blood. 1991; 78: 2708-14.

29- Folkesson H.G. et al. Acid aspiration-induced lung injury in rabbits is mediated by interleukin-8-dependent mechanisms. J Clin Invest. 1995; 96: 107-116.

30- Ley K. et al. Getting to the side of inflammation: the leukocyte adhesion cascade updates. Nat Rev Immunol. 2007; 7: 678-89.

31- Springer T.A. Traffic signal for lymphocyte recirculation and leukocyte emigration: the multistep paradigm. Cell. 1994; 76: 301-14.

32- McEver R.P. Selectins: lectins that initiate cell adhesion under flow. Curr Opin Cell Biol. 2002; 14: 581-6.

33- Martin T.R. et al. Effects of leukotriene B4 in the human lung: recruitment of neutrophils into the alveolar spaces without a change in protein permeability. J Clin Invest. 1989; 84: 1609-19.

34- Webster R.O. et al. Absence of inflammatory injury in rabbits challenged intravascularly with complement-derived chemotactic factors. Am Rev Respir Dis. 1982; 125: 335-40.

35- Downey G.P. et al. Regulation of neutrophil activation in acute lung injury. Chest. 1999; 116: S46-S54.

36- Alber A. et al. The role of macrophages in healing the wounded lung. Int J Exp Path. 2012; 93: 243-51.

37- Geissmann F. et al. Development of monocytes, macrophages, and dendritic cells. Science. 2010; 327: 656-61.

38- Pollard W. Trophic macrophages in development and disease. Nat Rev Immunol. 2009; 9: 259-70.

39- Mantovani A. et al. Macrophage polarization: tumor-associated macrophages as a paradigm for polarized M2 mononuclear phagocytes. Trends Immunol. 2002; 23: 549-55.

40- Gordon S. and Martinez F.O. Alternative activation of macrophages: mechanism and functions. Immunity. 2010; 32: 593-604.

41- Kreisel D. et al. In vivo two-photon imaging reveals monocyte-dependent neutrophil extravasation during pulmonary inflammation. Proc Natl Acad Sci. 2010; 107: 18073-8.

42- Reynolds H.Y. Lung inflammation and fibrosis: an alveolar macrophage-centered perspective from the 1970s to 1980s. Am J Respir Crit Care Med. 2005; 171: 98-102.

43- Dos Santos C.C. Advances in mechanisms of repair and remodelling in acute lung injury. Intensive Care Med. 2008; 34: 619-630.

44- Lewis J.F. and Jobe A.H. Surfactant and the acute respiratory distress syndrome. Am Rev Respir Dis. 1993; 147: 218-33.

45- Nkadi P.O. et al. An overview of pulmonary surfactant in the neonate: genetics, metabolism, and the role of surfactant in health and disease. Mol Genet Metab. 2009; 97: 95-101.

46- Gross N.J. et al. Separation of alveolar surfactant into subtypes. A comparison of methods. Am J Respir Crit Care Med. 2000; 162: 617-622.

47- Wright J.R. et al. Metabolism and turnover of lung surfactant. Am Rev Respir Dis. 1987; 136: 426-44.

48- Hartog A. et al. Comparison of exogenous surfactant therapy, mechanical ventilation with high end-expiratory pressure and partial liquid ventilation in a model of acute lung injury. Br J Anaesth. 1992; 82: 81-6.

49- Bosma K.J. et al. Pharmacotherapy for prevention and treatment of acute respiratory distress syndrome. Current and experimental approaches. Drugs. 2010; 70: 1255-82.

50- Sarrasague M.M. et al. Influence of serum protein and albumin addition on the structure and activity of an exogenous pulmonary surfactant. Respir Physiol Neurobiol. 2011; 175: 316-21.

51- Maruscak A.A. et al. Alterations to surfactant precede physiological deterioration during high tidal volume ventilation. Am J Physiol Lung Cell Mol Physiol. 2008; 294: L974-L983.

52- Simpson J. The alleged case of death from the action of chloroform. Lancet. 1848; 1: 175-175.

53- Mendelson C. The aspiration of stomach contents into the lungs during obstetric anesthesia. Am J Ostet Gynecol. 1946; 52:191-205.

54- Kennedy T.P. Acute acid aspiration lung injury in the rat: biphasic pathogenesis. Anest Analg. 1993; 77:754-60.

55- Marik P.E. Aspiration pneumonitis and aspiration pneumonia. N Engl J Med. 2001; 344: 665-71.

56- Knight P.R. The role of neutrophils, oxidants, and proteases in the pathogenesis of acid pulmonary injury. Anesthesiology. 1992; 77: 772-8.

57- Amigoni M. et al. Lung injury and recovery in a murine model of unilateral acid aspiration: functional, biochemical, and morphologic characterization. Anesthesiology 2008; 108: 1037-46

58- Milberg J.A. et al. Improved survival of patients with acute respiratory distress syndrome (ARDS): 1983-1993. JAMA. 1995; 273: 306-9.

59- Abel S.J.C. et al. Reduced mortality in association with the acute respiratory distress syndrome (ARDS). Thorax. 1998; 53: 292-4.

60- Pelosi P. et al. Prone position in acute respiratory distress syndrome. Eur Respir J. 2002; 20: 1017-28.

61- Walkey A.J. Acute respiratory distress syndrome: epidemiology and management approaches. Clin Epidemiol 2012; 4: 159-69.

62- Dellinger R.P. Effects of inhaled nitric oxide in patients with acute respiratory distress syndrome: results of a randomized phase II trial. Inhaled Nitric Oxide in ARDS Study Group. Crit Care Med. 1998; 26: 15-23.

63- Perkins G.D. et al. The beta-agonist lung injury trial (BALTI): a randomized placebo-controlled clinical trial. Am J Respir Crit Care Med. 2006; 173: 281-7

64- National Heart, Lung, and Blood Institute Acute Respiratory Distress Syndrome (ARDS) Clinical Trials Network. Randomized, placebo-controlled clinical trial of an aerosolized β2-agonist for treatment of acute lung injury. Am J Respir Crit Care Med. 2011; 184: 561-8.

65- Willson D.F. and Notter R.H. The future of exogenous surfactant therapy. Respir Care. 2011; 56: 1369-86.

66- Lewis J.F. Evoluation of exogenous surfactant treatment strategies in an adult model of acute lung injury. J Appl Physiol. 1996; 80: 1156-64

67- van Helden H.P.M. et al. Efficacy of Curosurf in a rat model of acute respiratory distress syndrome. Eur Respir J. 1998; 12: 533-9.

68- Scanziani M. et al. The effect of a single bolus of exogenous surfactant on lung compliance persists until two weeks after treatment in a model of acid aspiration pneumonitis. Pulm Pharmacol Ther. 2011; 24: 141-6.

69- Mittal N. et al. Intratracheal instillation of surfactant inhibits lipopolysaccharide-induced acute respiratory distress syndrome in rats. Am J Biomed Sci. 2010; 2: 190-201.

70- Walmrath D. et al. Bronchoscopic administration of bovine natural surfactant in ARDS and septic shock: impact on gas exchange and haemodynamics. Eur Respir J 2002; 19: 805-10.

71- Spragg R. et al. Acute effects of a single dose of porcine surfactant on patients with the adult respiratory distress syndrome. Chest. 1994; 105: 195-202.

72- Wiswell T.E. et al. Bronchopulmonary segmental lavage with Surfaxin (KL(4)-surfactant) for acute respiratory distress syndrome. Am J Respir Crit Care Med. 1999; 160: 1188-95.

73- Gregory T.J. et al. Bovine surfactant therapy for patients with acute respiratory distress syndrome. Am J Respir Crit Care Med. 1997; 155: 109-31.

74- Spragg R.G. et al. Effect of recombinant surfactant protein C-based surfactant on the acute respiratory distress syndrome. N Engl J Med. 2004; 351: 884-92

75- Anzueto A. Aerosolized surfactant in adults with sepsis-induced acute respiratory distress syndrome. N Engl J Med. 1996; 334: 1417-21

76- Kesecioglu J. Exogenous natural surfactant from treatment of acute lung injury and acute respiratory distress syndrome. Am J Respir Crit Care Med. 2009; 180: 989-94.

77- Mankoff D.M. A definition of molecular imaging. J Nucl Med. 2007; 48: 18N-19N.

78- Bellani G. et al. Imaging in acute lung injury and acute respiratory distress syndrome. Curr Opin Crit Care. 2012; 18: 29-34.

79- Chen L. D. and NìKinahan P.E. Multimodality molecular imaging of the lung. J Magn Reson Imaging. 2010; 32: 1409-20.

80- Schuster D.P. et al. Recent advances in imaging the lungs of intact small animals. Am J Respir Cell Mol Biol. 2004; 30: 129-38.

81- Ford N.L. et al. Fundamental image quality limits for microcomputed tomography in small animals. Med Phys. 2003; 30: 2869-77.

82- Johnson K.A. Imaging techniques for small animal imaging models of pulmonary disease: micro-CT. Toxicol Pathol. 2007; 35: 59-64.

83- Schambach S.J. et al. Application of micro-CT in small animal imaging. Methods. 2010; 50: 2-13.

84- Walters E.B. et al. Improved method of in vivo respiratory-gated micro-CT imaging. Phys Med Biol. 2004; 49: 4163-72.

85- Hoffman E.A. et al. Characterization of the interstitial lung diseases via density-based and texture-based analysis of computed tomography images of lung structure and function. Acad Radiol. 2003; 10: 1104-18

86- Gattinoni L. et al. Morphological response to positive end expiratory pressure in acute respiratory failure. Intensive Care Med. 1986; 12: 137-42.

87- Bruhn A. et al. Tidal volume is a major determinant of cyclic recruitment-derecruitment in acute respiratory distress syndrome. Minerva Anestesiol. 2011; 77: 418-26.

88- Protti A. et al. Lung stress and strain during mechanical ventilation: any safe threshold? Am J Respir Crit Care Med. 2011; 183: 1354-62.

89- Caironi P. et al. Lung opening and closing during ventilation of acute respiratory distress syndrome. Am J Respir Crit Care Med. 2010; 181: 578-86.

90- Gattinoni L. et al. Body position changes redistribute lung computed-tomographic density in patients with acute respiratory failure. Anesthesiology. 1991; 74: 15-23

91- Lu Q. et al. Computed tomography assessment of exogenous surfactant-induced lung reaeration in patients with acute lung injury. Crit Care. 2010; 14: R135.

92- Dakin J. et al. Changes in lung composition and regional perfusion and tissue distribution in patients with ARDS. Respirology. 2011; 16: 1265-75.

93- Mull R.T. Mass estimates by computed tomography: physical density from CT numbers. AJR Am J Roentgenol. 1984; 143: 1101-04.

94- Gattinoni L. et al. Relationship between lung computed tomography density, gas exchange, and PEEP in acute respiratory failure. Anesthesiology. 1988; 69: 824-32.

95- Pelosi P. et al. Recruitment and derecruitment during acute respiratory failure: an experimental study. Am J Respir Crit Care Med. 2001; 164: 122-30.

96- Saleem A et al. Clinical molecular imaging with positron emission tomography. Eur J Cancer. 2006; 42: 1720-7.

97- Zavala F. and Lenfant M. Benzodiasepines and PK 11195 exert immunomodulating activities on a specific receptor on macrophages. Ann NY Acad Sci. 1987; 96: 240-9.

98- Hatori A. et al. PET imaging of lung inflammation with [18F]FEDAC, a radioligand for translocator protein (18kDa). PLOS one. 2012; 7: e45065.

99- de Prost N. et al. Assessment of lung inflammation with 18F-FDG PET during acute lung injury. AJR Am J Roentgenol. 2010; 195: 292-300.

100-   Zhou Z. et al. Molecular imaging of lung glucose uptake after endotoxin in mice. Am J Physiol Lung Cell Mol Physiol. 2005; 289: L760-L768.

101-   Tsuchida T. et al. Noninvasive measurement of cerebral metabolic rate of glucose using standardized input function. J Nucl Med. 1999; 40: 1441-5

102-   Boellaard R. Standards for PET image acquisition and quantitative data analysis. J Nucl Med. 2009; 50: 11S-20S.

103-   Jones H. et al. Dissociation of neutrophil emigration and metabolic activity in lobar pneumonia and bronchiectasis. Eur Respir J. 1997; 10: 795-803.

104-   Chen D.L. et al. Quantifying pulmonary inflammation in cystic fibrosis with positron emission tomography. Am J Respir Crit Care Med. 2006; 173: 1363-9.

105-   Jones H.A. et al. In vivo assessment of lung inflammatory cell activity in patients with COPD and asthma. Eur Respir J. 2003; 21: 567-73.

106-   Chen D.L. et al. Positron emission tomography with [18F]fluorodeoxyglucose to evaluate neutrophil kinetics during acute lung injury. Am J Physiol Lung Cell Mol Physiol. 2004; 286: L834-840.

107-   Jones H.A. et al. In vivo measurement of neutrophil activity in experimental lung inflammation. Am J Respir Crit Care Med. 1994; 149: 1635-9.

108-   Musch G. et al. Regional gas exchange and cellular metabolic activity in ventilator-induced lung injury. Anesthesiology. 2007; 106: 723-35.

109-   Phelps M.E. et al. Investigation of [18F]FDG for the measure of myocardial glucose metabolism. J Nucl Med. 1978; 19: 1311-19.

110-   Reutershan J. et al. Sequential recruitment of neutrophils into lung and bronchoalveolar lavage fluid in LPS-induced acute lung injury. Am J Physiol Lung Cell Mol Physiol. 2005; 298: L807-L815.

111-   Reiss M. and Roos D. Differences in oxygen metabolism of phagocytosing monocytes and neutrophils. J Clin Invest. 1978; 61: 480-8.

112-   Deichen J.T. et al. Uptake of [18F]fluorodeoxyglucose in human monocyte-macrophages in vitro. Eur J Nucl Med Mol Imaging. 2003; 30: 267-73.

113-   Jones H.A. et al. Pulmonary fibrosis correlates with duration of tissue neutrophil activation. Am J Respir Crit Care Med. 1998; 158: 620-8.

114-   Rodrigues R.S. et al. FDG-PET in patients at risk for acute respiratory distress syndrome: a preliminary report. Intensive Care Med. 2008; 34: 2273-8.

115-   Pawlik M.T- et al. Hydrochloric acid aspiration increases right ventricular systolic pressure in rats. Eur J Anaesthesiology. 2009; 26: 285-92.

116-   Jones H.A. et al. Kinetics of lung macrophages monitored in vivo following particulate challenge in rabbits. Toxicol Appl Pharmacol. 2002; 183: 46-54.

117-   Branley H.M. et al. Peripheral-type benzodiazepine receptors in bronchoalveolar lavage cells of patients with interstitial lung disease. Nucl Med Biol. 2007; 34: 553-8.